gene system in 293 cells. As shown in Figure 3, our Atelocollagen-mediated siRNA delivery technology exhibited an inhibitory effect as efficient as that in the conventional liposome transfer method.

In the next experiment, we employed human testicular tumor cells, NEC8, which showed high levels of HST-1/FGF-4 mRNA expression (17) and specifically inhibited cell growth by suppression of HST-1/FGF-4 (19). An Atelocollagen-mediated delivery of human HST-1/FGF-4 siRNA was performed to inhibit NEC8 cell growth. The inhibitory effect of HST-1/FGF-4 siRNA was dose-dependent and 1.4 μg per 3.5×10^4 cells produced maximum inhibition (Figure 4A). At a dose of 1.4 μg per 3.5×10^4 cells showed ~10% toxicity by the trypan blue exclusion. Therefore, we used human HST-1/FGF-4 siRNA at a submaximal dose of 0.7 μg per 3.5×10^4 NEC8 cells for further studies. The NEC8 cells transfected with siRNA plus polycation reagent showed an inhibitory effect for maximum of 4 days post-transfection and there was no inhibition of cell growth thereafter (Figure 4B). In addition, siRNA alone and liposome alone showed no significant inhibitory effect (data not shown). In contrast, HST-1/FGF-4 siRNA complexed with Atelocollagen displayed inhibition of cell growth for at least 7 days in culture. To verify further that cell growth inhibition reflected a gene-specific silencing event, HST-1/FGF-4 protein production in NEC8 cells was investigated by ELISA (20). As shown in Figure 5, HST-1/FGF-4 protein levels were significantly inhibited when cells were transfected with the siRNA/Atelocollagen complex. Taken together, these data show that the Atelocollagen stabilized siRNA and thereby siRNA/Atelocollagen complex was able to produce an efficient and a long-term gene silencing effect *in vitro*.

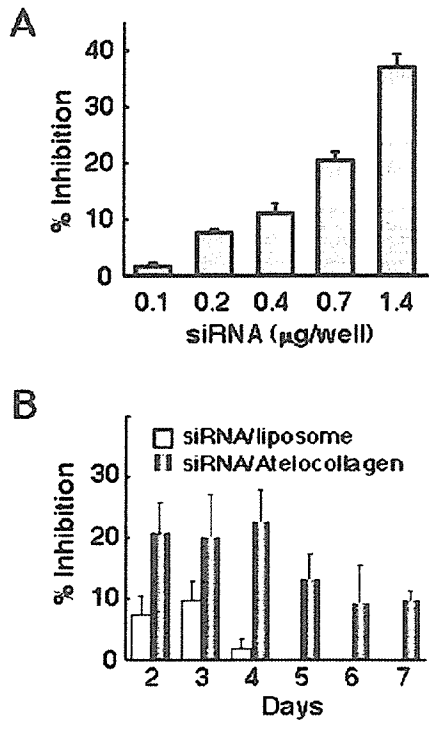

Figure 4. Inhibition of human testicular tumor cell growth by siRNA/Atelocollagen complex. (**A**) Dose-dependent inhibition of NEC8 cell growth. Human HST-1/FGF-4 siRNAs (0.1–1.4 μg) complexed with 0.008% Atelocollagen were transduced into NEC8 cells. Cell proliferation was measured at 2 days after treatment ($n = 4$, mean ± SE). (**B**) Long-term inhibition of NEC8 cell growth by siRNA/Atelocollagen complex. HST-1/FGF-4 siRNA (0.7 μg) was transfected into NEC8 cells by polycation-reagent and complexed with 0.008% Atelocollagen ($n = 6$, mean ± SE).

Enhanced gene silencing by siRNA/Atelocollagen complex *in vivo*

To test whether Atelocollagen-mediated siRNA transfer is valid for gene silencing *in vivo* (Figure 1), animal experiments were performed on mice bearing a luciferase-producing melanoma. Non-invasive *in vivo* bioluminescence imaging analysis showed that luciferase expressions in the tumor of mice injected with GL3 siRNA alone and liposome-complexed siRNA were maximally inhibited at 2–3 days after injection, and increased thereafter. In contrast, mice administered with the siRNA/Atelocollagen complex showed a relatively strong and sustained inhibition of luciferase expression *in vivo* (Figures 6A and B). As previously shown, radiolabeled siRNA mixed with Atelocollagen existed in the tumors for at least a week and remained intact (21). These results suggest that an Atelocollagen-mediated *in vivo* transfer of siRNA could be a powerful and simple method to study loss-of-function of genes in animals.

Inhibition of tumor growth by siRNA/Atelocollagen complex

Testicular injections of NEC8 cell lines in Balb/c nude mice demonstrated relevant tumor biology (19). In this study, the NEC8 cell line was labeled through expression of a stable integrant of the luciferase gene. Athymic nude mice laden

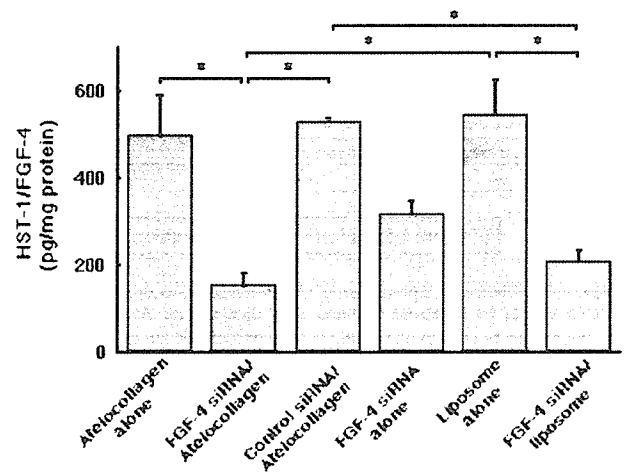

Figure 5. Silencing effect on HST-1/FGF-4 protein production in NEC8 cells. HST-1/FGF-4 siRNA (0.7 μg) complexed with 0.008% Atelocollagen was transduced into NEC8 cells. As a control, an Atelocollagen complex with non-specific control siRNA duplex that shows no silencing effect on human HST-1/FGF-4 was used (control-siRNA/Atelocollagen). Production of HST-1/FGF-4 protein was measured by ELISA 3 days after the transfer of siRNA ($n = 3$, mean ± SE). *, $P < 0.05$.

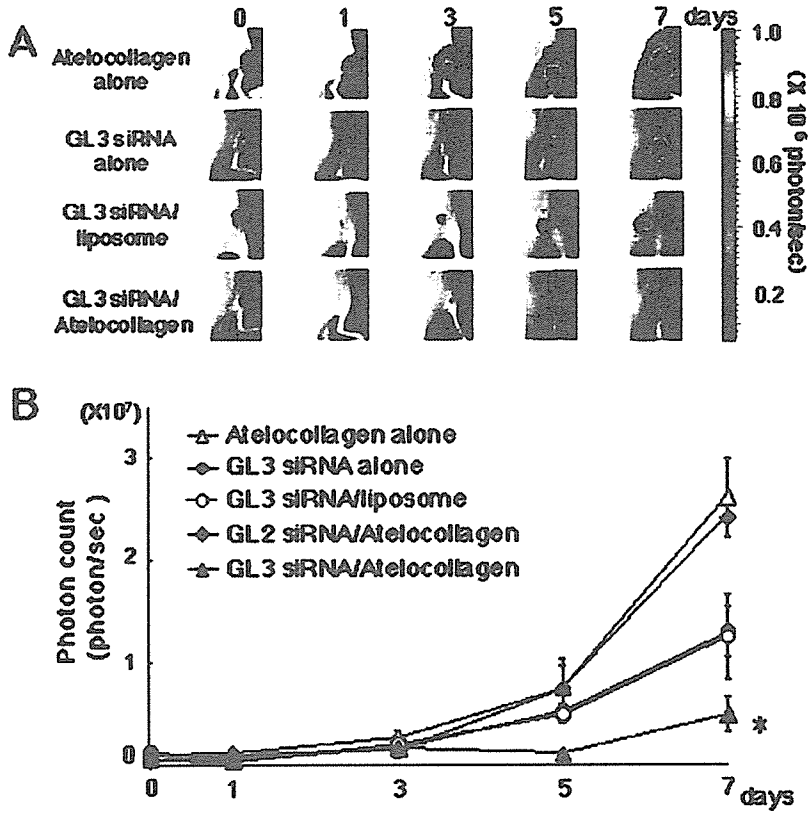

Figure 6. *In vivo* imaging of gene silencing effect of siRNA/Atelocollagen complex. (A) Luciferase GL3 siRNA (2.5 μg) complexed with 0.5% Atelocollagen was administered into mice and luciferase expression of xenografted tumors was monitored by *in vivo* imaging analysis. As a control, mice administered with siRNA alone, siRNA complexed with liposome and Atelocollagen alone were investigated. Color bar represents signal intensity code over body surface area. (B) Luciferase gene expression was measured periodically and is represented as photon/s. Number of tumors at each time point is 4. As a control for GL3 siRNA, GL2 siRNA was used. Data represent the mean ± SE. *, $P < 0.05$ versus Atelocollagen treatment.

with a testicular injection of NEC8-luc cells were randomly selected for treatment with HST-1/FGF-4 siRNA alone, siRNA complexed with Atelocollagen or Atelocollagen alone. Previously, bioluminescence imaging of orthotopic xenografts in mice demonstrated a linear correlation between tumor bioluminescence and tumor volume (18,22). Tumor growth was inhibited by treatment with human HST-1/FGF-4 siRNA complexed with Atelocollagen. At 21 days following treatment, tumor volume in mice treated with siRNA complexed with Atelocollagen was smaller than that in the control mice treated with Atelocollagen alone (Figure 7A and B). In contrast, tumors treated with siRNA alone and control siRNA/Atelocollagen showed no significant volume reduction. Furthermore, the FGF-4 siRNA/Atelocollagen complex significantly inhibited the production of FGF-4 in the tumors (Figure 7C) and this inhibition lasted for 20 days. Therefore, the Atelocollagen-mediated siRNA transfer is a significant novel method for inhibition of tumor growth *in vivo*.

DISCUSSION

Silencing of gene expression by siRNAs is rapidly becoming a powerful tool for the genetic analysis of a wide variety of mammalian cells. Although in the original studies, the expression of siRNA in mammalian cells was achieved via the transfection of double-stranded oligonucleotides, subsequent studies described the limited duration of the gene silencing effect. To overcome this problem, the use of plasmids to achieve a long-term and stable expression of siRNA was established (23–25). In addition, several groups have described the use of adenoviral vectors (9), retroviral vectors (26) and self-inactivating lentiviral vectors (27) for siRNA delivery. However, viral vectors suffer from the problem of severe side effects. Although the 'hydrodynamic transfection method' and a liposome transfection method were recently reported for siRNA delivery into animals (8,28), none is suitable for clinical use. Therefore, the development of safe non-vector-based siRNA delivery systems is critical for the future of siRNA-based therapies. Here, we used an Atelocollagen-mediated siRNA transfer in an *in vitro* and *in vivo* germ cell tumor-suppression model. Because Atelocollagen allowed increased cellular uptake, nuclease resistance and prolonged release of siRNAs, Atelocollagen complexed with siRNA rather than siRNA alone or a polycation transfer method resulted in stronger gene silencing effects over other methods. It is known that Atelocollagen has the ability to transfer genes to both dividing and non-dividing

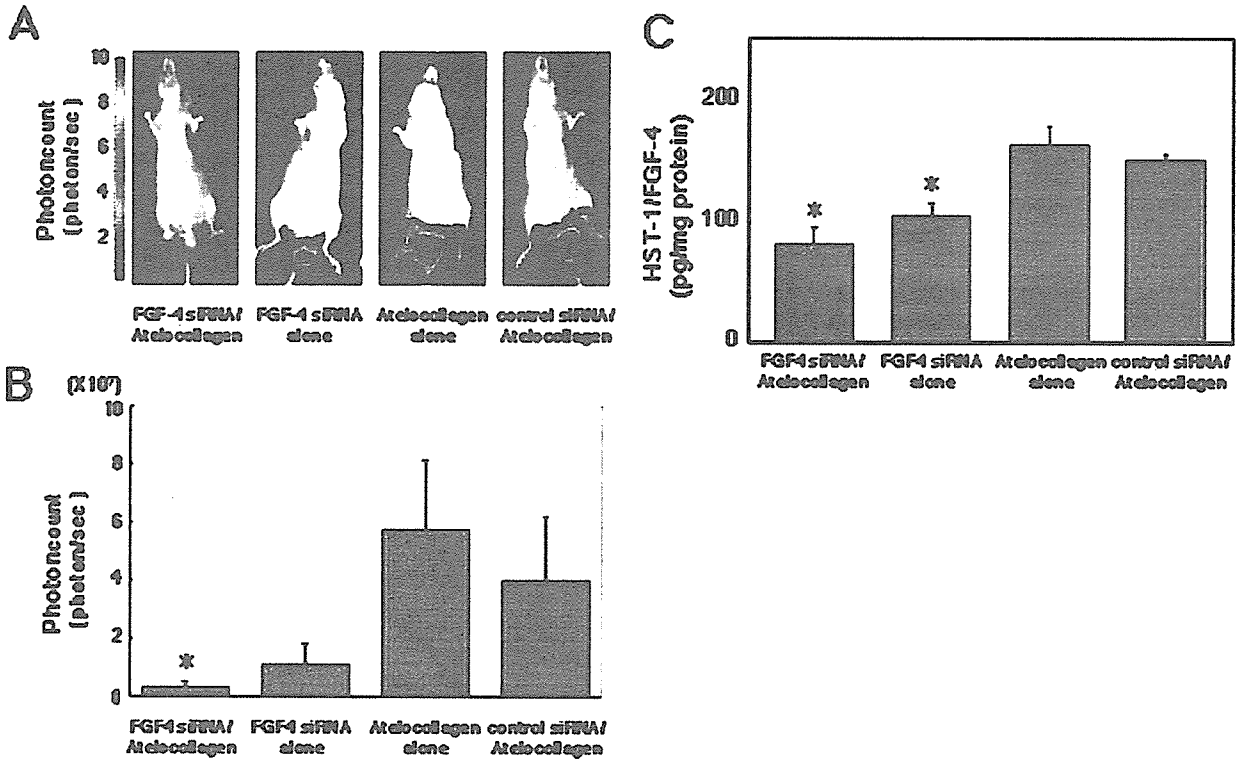

Figure 7. Effect of siRNA/Atelocollagen complex on the growth of a xenograft tumor. (A) Human HST-1/FGF-4 siRNA (2.5 μg) complexed with 0.5% Atelocollagen was transduced into an orthotopic germ cell tumor of NEC8 cells expressing the luciferase gene. Representative images at 21 days after treatment are shown. As a control, an Atelocollagen complex with non-specific control siRNA duplex that shows no silencing effect on human HST-1/FGF-4 was used (control siRNA/Atelocollagen). (B) Measurements of a xenograft tumor bioluminescence at 21 days after treatment. Data represent the mean ± SE. *, $P < 0.05$ versus Atelocollagen alone treatment. (C) Evaluation of HST-1/FGF-4 protein expression in tumor tissue extracts 3 days after treatment. Protein levels were quantified by ELISA. Data represent the mean ($n = 4$) ± SE. *, $P < 0.05$ versus Atelocollagen alone and control siRNA/Atelocollagen treatment.

cells. Thus, for clinical applications in RNAi therapy, an Atelocollagen-based siRNA transfer system represents an attractive method to achieve maximal function of siRNA-based gene silencing *in vivo*.

One technical problem associated with siRNA transfer *in vivo* is the targeting of siRNA delivery to a specific tissue. For this purpose, our Atelocollagen-based transfer method has great potential for site-specific transportation of target siRNAs because the complex of siRNA/Atelocollagen becomes solid when transplanted and remains so for a defined period *in vivo*. In addition, an Atelocollagen complex can be delivered as micro-particles for intravenous injection, making systemic delivery of siRNA possible. A recent report showed the potential for Atelocollagen-mediated systemic antisense therapeutics for inflammatory disease (29). Following *in vivo* administration, the incorporated siRNAs are slowly released over an extended period of time. This eliminates the need for multiple injections of siRNA and siRNA vectors, in lessened side effects.

Although siRNAs are thought to be too short to induce interferon expression, recent reports has shown that siRNA sequences and their method of delivery may trigger an interferon response (30,31). Therefore, alternative strategies are needed to reduce the induction of non-specific side effects. In this regard, our Atelocollagen-mediated non-vector transfer method is an attractive strategy to deliver siRNAs *in vivo*, since our Atelocollagen has low-toxicity and is low-immunogenic, and hence unlikely to stimulate interferon expression *in vivo*.

Finally, based on the ability of Atelocollagen to achieve the sustained release of siRNA and to enhance the stability of siRNA *in vivo*, our novel delivery method demonstrates potential for use as a therapeutic tool for the delivery of siRNA.

ACKNOWLEDGEMENTS

We thank Ms Kazumi Kimura, Ms Masako Hosoda and Ms Ayako Inoue for their excellent technical work. This work was supported in part by a Grant-in-Aid for the Second-Term Comprehensive 10-Year Strategy for Cancer Control, Health Science Research Grants for the Research on the Human Genome and Gene Therapy from the Ministry of Health, Labour and Welfare of Japan, a Grant-in-Aid for Scientific Research on Priority Areas Cancer from the Ministry of Education, Culture, Sports, Science and Technology, and the Program for Promotion of Fundamental Studies in Health Sciences of the Organization for Pharmaceutical Safety and Research of Japan.

REFERENCES

1. Fire,A., Xu,S., Montgomery,M.K., Kostas,S.A., Driver,S.E. and Mello,C.C. (1998) Potent and specific genetic interference by double-stranded RNA in *Caenorhabditis elegans*. *Nature*, **391**, 806–811.
2. Scherr,M., Morgan,M.A. and Eder,M. (2003) Gene silencing mediated by small interfering RNAs in mammalian cells. *Curr. Med. Chem.*, **10**, 245–256.
3. Elbashir,S.M., Harborth,J., Lendeckel,W., Yalcin,A., Weber,K. and Tuschl,T. (2001) Duplexes of 21-nucleotide RNAs mediate RNA interference in cultured mammalian cells. *Nature*, **411**, 494–498.
4. Lee,N.S., Dohjima,T., Bauer,G., Li,H., Li,M.J., Ehsani,A., Salvaterra,P. and Rossi,J. (2002) Expression of small interfering RNAs targeted against HIV-1 rev transcripts in human cells. *Nat. Biotechnol.*, **20**, 500–505.
5. Paul,C.P., Good,P.D., Winer,I. and Engelke,D.R. (2002) Effective expression of small interfering RNA in human cells. *Nat. Biotechnol.*, **20**, 505–508.
6. Simeoni,F., Morris,M.C., Heitz,F. and Divita,G. (2003) Insight into the mechanism of the peptide-based gene delivery system MPG: implications for delivery of siRNA into mammalian cells. *Nucleic Acids Res.*, **31**, 2717–2724.
7. Bertrand,J.R., Pottier,M., Vekris,A., Opolon,P., Maksimenko,A. and Malvy,C. (2002) Comparison of antisense oligonucleotides and siRNAs in cell culture and *in vivo*. *Biochem. Biophys. Res. Commun.*, **296**, 1000–1004.
8. Sorensen,D.R., Leirdal,M. and Sioud,M. (2003) Gene silencing by systemic delivery of synthetic siRNAs in adult mice. *J. Mol. Biol.*, **327**, 761–766.
9. Xia,H., Mao,Q., Paulson,H.L. and Davidson,B.L. (2002) siRNA-mediated gene silencing *in vitro* and *in vivo*. *Nat. Biotechnol.*, **20**, 1006–1010.
10. Tomar,R.S., Matta,H. and Chaudhary,P.M. (2003) Use of adeno-associated viral vector for delivery of small interfering RNA. *Oncogene*, **22**, 5712–5715.
11. Matta,H., Hozayev,B., Tomar,R., Chugh,P. and Chaudhary,P.M. (2003) Use of lentiviral vectors for delivery of small interfering RNA. *Cancer Biol. Ther.*, **2**, 206–210.
12. Stenzel,K.H., Miyata,T. and Rubin,A.L. (1974) Collagen as a biomaterial. *Annu. Rev. Biophys. Bioeng.*, **3**, 231–253.
13. Ochiya,T., Nagahara,S., Sano,A., Itoh,H. and Terada,M. (2001) Biomaterials for gene delivery: atelocollagen-mediated controlled release of molecular medicines. *Curr. Gene Ther.*, **1**, 31–52.
14. Honma,K., Ochiya,T., Nagahara,S., Sano,A., Yamamoto,H., Hirai,K., Aso,Y. and Terada,M. (2001) Atelocollagen-based gene transfer in cells allows high-throughput screening of gene functions. *Biochem. Biophys. Res. Commun.*, **289**, 1075–1081.
15. Ochiya,T., Takahama,Y., Nagahara,S., Sumita,Y., Hisada,A., Itoh,H., Nagai,Y. and Terada,M. (1999) New delivery system for plasmid DNA *in vivo* using atelocollagen as a carrier material: the Minipellet. *Nature Med.*, **5**, 707–710.
16. Sano,A., Maeda,M., Nagahara,S., Ochiya,T., Honma,K., Itoh,H., Miyata,T. and Fujioka,K. (2003) Atelocollagen for protein and gene delivery. *Adv. Drug Deliv. Rev.*, **55**, 1651–1677.
17. Yoshida,T., Tsutsumi,M., Sakamoto,H., Miyagawa,K., Teshima,S., Sugimura,T. and Terada,M. (1988) Expression of the HST1 oncogene in human germ cell tumors. *Biochem. Biophys. Res. Commun.*, **155**, 1324–1329.
18. Vooijs,M., Jonkers,J., Lyons,S. and Berns,A. (2002) Noninvasive imaging of spontaneous retinoblastoma pathway-dependent tumors in mice. *Cancer Res.*, **62**, 1862–1867.
19. Hirai,K., Sasaki,H., Sakamoto,H., Takeshita,F., Asano,K., Kubota,Y., Ochiya,T. and Terada,M. (2003) Antisense oligodeoxynucleotide against HST-1/FGF-4 suppresses tumorigenicity of an orthotopic model for human germ cell tumor in nude mice. *J. Gene Med.*, **5**, 951–957.
20. Konishi,H., Ochiya,T., Sakamoto,H., Tsukamoto,M., Saito,I., Muto,T., Sugimura,T. and Terada,M. (1995) Effective prevention of thrombocytopenia in mice using adenovirus-mediated transfer of HST-1 (FGF-4) gene. *J. Clin. Invest.*, **96**, 1125–1130.
21. Takei,Y., Kadomatsu,K., Yuzawa,Y., Matsuo,S. and Muramatsu,T. (2004) A small interfering RNA targeting vascular endothelial growth factor as cancer therapeutics. *Cancer Res.*, **64**, 3365–3370.
22. Rehemtulla,A., Stegman,L.D., Cardozo,S.J., Gupta,S., Hall,D.E., Contag,C.H. and Ross,B.D. (2000) Rapid and quantitative assessment of cancer treatment response using *in vivo* bioluminescence imaging. *Neoplasia*, **2**, 491–495.
23. Miyagishi,M. and Taira,K. (2002) U6 promoter-driven siRNAs with four uridine 3′ overhangs efficiently suppress targeted gene expression in mammalian cells. *Nat. Biotechnol.*, **20**, 497–500.
24. Hasuwa,H., Kaseda,K., Einarsdottir,T. and Okabe,M. (2002) Small interfering RNA and gene silencing in transgenic mice and rats. *FEBS Lett.*, **532**, 227–230.
25. Pekarik,V., Bourikas,D., Miglino,N., Joset,P., Preiswerk,S. and Stoeckli,E.T. (2003) Screening for gene function in chicken embryo using RNAi and electroporation. *Nat. Biotechnol.*, **21**, 93–96.
26. Hemann,M.T., Fridman,J.S., Zilfou,J.T., Hernando,E., Paddison,P.J., Cordon-Cardo,C., Hannon,G.J. and Lowe,S.W. (2003) An epi-allelic series of p53 hypomorphs created by stable RNAi produces distinct tumor phenotypes *in vivo*. *Nature Genet.*, **33**, 396–400.
27. Rubinson,D.A., Dillon,C.P., Kwiatkowski,A.V., Sievers,C., Yang,L., Kopinja,J., Rooney,D.L., Ihrig,M.M., McManus,M.T., Gertler,F.B. *et al.* (2003) A lentivirus-based system to functionally silence genes in primary mammalian cells, stem cells and transgenic mice by RNA interference. *Nature Genet.*, **33**, 401–406.
28. Song,E., Lee,S.K., Wang,J., Ince,N., Ouyang,N., Min,J., Chen,J., Shankar,P. and Lieberman,J. (2003) RNA interference targeting Fas protects mice from fulminant hepatitis. *Nature Med.*, **9**, 347–351.
29. Hanai,K., Kurokawa,T., Minakuchi,Y., Maeda,M., Nagahara,S., Ito,H., Ochiya,T. and Sano,A. (2004) Potential for atelocollagen-mediated systemic antisense therapeutics for inflammatory disease. *Human Gene Ther.*, **15**, 263–272.
30. Bridge,A.J., Pebernard,S., Ducraux,A., Nicoulaz,A.L. and Iggo,R. (2003) Induction of an interferon response by RNAi vectors in mammalian cells. *Nature Genet.*, **34**, 263–264.
31. Sledz,C.A., Holko,M., de Veer,M.J., Silverman,R.H. and Williams,B.R. (2003) Activation of the interferon system by short-interfering RNAs. *Nature Cell Biol.*, **5**, 834–839.

Preparation and Characterization of Polyion Complex Micelles with a Novel Thermosensitive Poly(2-isopropyl-2-oxazoline) Shell via the Complexation of Oppositely Charged Block Ionomers†

Joon-Sik Park,‡ Yoshitsugu Akiyama,§ Yuichi Yamasaki,‡,|| and Kazunori Kataoka*,‡,||,⊥

Department of Materials Engineering, Graduate School of Engineering, The University of Tokyo, 7-3-1 Hongo, Bunkyo-ku, Tokyo 113-8656, Japan, Departments of Chemistry and Biology, University of Virginia, McCormick Road, Charlottesville, Virginia 22904, Center for NanoBio Integration, The University of Tokyo, 7-3-1 Hongo, Bunkyo-ku, Tokyo 113-8656, Japan, and Center for Disease Biology and Integrative Medicine, Graduate School of Medicine, The University of Tokyo, 7-3-1 Hongo, Bunkyo-ku, Tokyo 113-0033, Japan

Received May 22, 2006. In Final Form: September 5, 2006

Novel thermosensitive polyion complex (PIC) micelles were prepared in an aqueous medium based on the complexation of a pair of oppositely charged block ionomers, poly(2-isopropyl-2-oxazoline)-*b*-poly(amino acid)s (P*i*PrOx-*b*-PAA), containing thermosensitive P*i*PrOx segments. The controlled synthesis of P*i*PrOx-*b*-PAA was achieved via the ring-opening anionic polymerization of *N*-carboxyanhydrides (NCA) of either ϵ-benzyloxycarbonyl-L-lysine (Lys(Z)-NCA) or β-benzyl-L-aspartate (BLA-NCA) with ω-amino-functionalized P*i*PrOx macroinitiators and the subsequent deprotection reaction under acidic or basic conditions. Gel permeation chromatography (GPC) and ^{1}H NMR spectroscopy revealed that the syntheses of two block ionomers, poly(2-isopropyl-2-oxazoline)-*b*-poly(L-lysine) [P*i*PrOx-P(Lys)] and poly(2-isopropyl-2-oxazoline)-*b*-poly(aspartic acid) [P*i*PrOx-P(Asp)], proceeded almost quantitatively to give samples with a narrow molecular weight distribution ($M_w/M_n \leq 1.2$). The mixing of these two oppositely charged block ionomers in an aqueous medium led to the spontaneous formation of PIC micelles, which was confirmed by dynamic light scattering (DLS) and transmission electron microscopy (TEM). The PIC micelles were spherical particles with a narrow distribution in the range of the measured concentration (0.125−1 mg/mL) and were stable without any secondary aggregates. Furthermore, the PIC micelles had a constant cloud-point temperature (T_{cp}) of ~32 °C under physiological conditions regardless of the total concentration, suggesting that the concentration factor is almost negligible with respect to the T_{cp} of the micelles presumably because of the increased local concentration of the P*i*PrOx segments in the shell layer. These PIC micelles have a promising application as a size-regulated smart nanocontainer loading charged compounds as well as bearing a thermosensitive outer shell that is useful for physical affinity control.

Introduction

Recently, the self-assemblies of block copolymers have attracted an enormous amount of interest as potential materials in separation technology[1] and surface modification[2] and have promising carriers in drug delivery systems.[3,4] In particular, the use of polymeric micelles as drug carriers has numerous advantages[3] resulting from structural characteristics such as mesoscopic-scale size, core−shell structure, and thermodynamic stability. In particular, the polyion complex (PIC) micelles have opened the way to incorporate charged macromolecules of synthetic and biological origins, including proteins and nucleic acids, into the micelles.[5] The cores of PIC micelles could serve as nanoreservoirs for these charged compounds, allowing control of innate properties such as stability, solubility, and reactivity. A fundamental study of PIC micelle formation from a mixture of a series of oppositely charged block ionomers with poly(ethylene glycol) (PEG) as a hydrophilic segment, poly(ethylene glycol)-*b*-poly(L-lysine) [PEG-P(Lys)], and poly(ethylene glycol)-*b*-poly(aspartic acid) [PEG-P(Asp)] even revealed a unique molecular recognition process based on the length of the charged segments.[6] The PIC micelles entrapping enzymes in the core were also expected to be useful as functional materials such as nanometric-scale enzymatic reactors, which might be useful in the field of diagnostics and therapeutics.[7]

These interesting properties of PIC micelles as a functional supramolecular assembly may be enhanced when combined with a responsivity to external chemical and physical stimuli such as pH, magnetism, light, and heat. Of particular interest is the thermoresponsivity that can be a useful function in various applications including thermosensitive nanoreactors and drug delivery systems. Although there have been several studies on thermosensitive polymeric micelles with the potential to be a

† Part of the Stimuli-Responsive Materials: Polymers, Colloids, and Multicomponent Systems special issue.

* To whom correspondence should be addressed. E-mail: kataoka@bmw.t.u-tokyo.ac.jp. Tel: +81-3-5841-7138. Fax: +81-3-5841-7139.

‡ Department of Materials Engineering, Graduate School of Engineering, The University of Tokyo.

§ University of Virginia.

|| Center for NanoBio Integration, The University of Tokyo.

⊥ Center for Disease Biology and Integrative Medicine, Graduate School of Medicine, The University of Tokyo.

(1) (a) Nagarajan, R.; Barry, M.; Ruckenstein, E. *Langmuir* **1986**, *2*, 210. (b) Hurter, P. N.; Hatton, T. A. *Langmuir* **1992**, *8*, 1291.

(2) (a) Webber, S. E. *J. Phys. Chem.* **1998**, *102*, 2618. (b) Emoto, K.; Iijima, M.; Nagasaki, Y.; Kataoka, K. *J. Am. Chem. Soc.* **2000**, *122*, 2653. (c) Otsuka, H.; Nagasaki, Y.; Kataoka, K. *Curr. Opin. Colloid Interface Sci.* **2001**, *6*, 21.

(3) (a) Kataoka, K.; Kwon, G. S.; Yokoyama, M.; Okano, T.; Sakurai, Y. *J. Controlled Release* **1993**, *24*, 119. (b) Kataoka, K.; Harada, A.; Nagasaki, Y. *Adv. Drug Delivery Rev.* **2001**, *47*, 113. (c) Nishiyama, N.; Bae, Y. S.; Miyata, K.; Fukushima, S.; Kataoka, K. *Drug Discovery Today* **2005**, 2, 21.

(4) (a) Discher, D. E.; Eisenberg. A. *Science* **2002**, *297*, 967. (b) Discher, B. M.; Hammer, D. A.; Bates, F. S.; Discher, D. E. *Curr. Opin. Colloid Interface Sci.* **2000**, *5*, 125.

(5) (a) Harada, A.; Kataoka, K. *Macromolecules* **1995**, *28*, 5294. (b) Kabanov, A. V.; Bronich, T. K.; Kabanov, V. A.; Yu, K.; Eisenberg, A. *Macromolecules* **1996**, *29*, 6797. (c) Kakizawa, Y.; Kataoka, K. *Adv. Drug Delivery Rev.* **2002**, *54*, 203.

(6) (a) Harada, A.; Kataoka, K. *Science* **1999**, *283*, 65. (b) Harada, A.; Kataoka, K. *Macromolecules* **2003**, *36*, 4995.

(7) (a) Harada, A.; Kataoka, K. *Macromolecules* **1998**, *31*, 288. (b) Harada, A.; Kataoka, K. *J. Am. Chem. Soc.* **1999**, *121*, 9241. (c) Harada, A.; Kataoka, K. *J. Am. Chem. Soc.* **2003**, *125*, 15306. (d) Jaturanpinyo, M.; Harada, A.; Yuan, X.; Kataoka, K. *Bioconjugate Chem.* **2004**, *15*, 344.

10.1021/la061431j CCC: $37.00
Published on Web 11/10/2006

Scheme 1. Syntheses of Block Copolymers (P*i*PrOx-P(Lys(Z)) and P*i*PrOx-PBLA) and Deprotected Block Ionomers (P*i*PrOx-P(Lys) and P*i*PrOx-P(Asp))

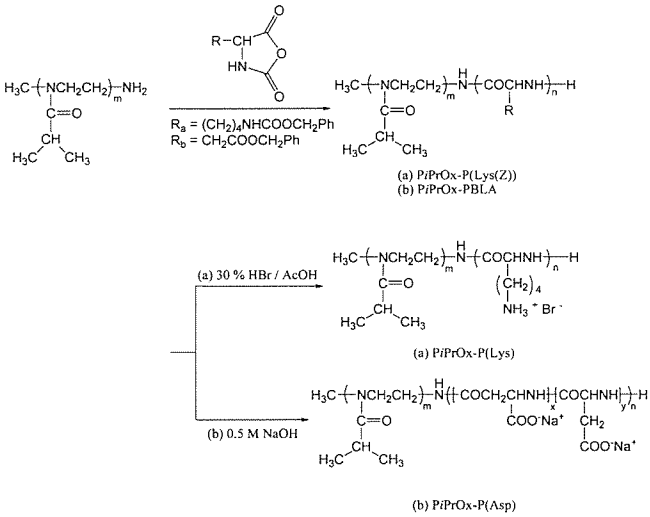

site-specific drug carrier based on poly(*N*-isopropylacrylamide) (PNIPAAm),[8] they have focused on the modulated amphiphilicity required to form the micelle with a hydrophobic inner core that is useful for the entrapment of hydrophobic therapeutic molecules such as anticancer drugs.[9] Little attention has been paid to the PIC micelles bearing a thermosensitive shell layer, though they have become even more attractive as an intelligent carrier of charged compounds utilizing temperature changes.

Of importance to the construction of PIC micelles with clear thermosensitivity are block ionomers composed of a hydrophilic segment with regulated thermosensitivity. In this regard, our recent findings of the quantitative cationic polymerization and selective end-functionalization of novel thermosensitive poly-(2-isopropyl-2-oxazoline) (P*i*PrOx) telechelics are attractive.[10] The polymerization proceeded in a good controlled manner under optimum temperature conditions with appreciably narrow molecular weight distributions ($M_w/M_n \leq 1.03$). In particular, ω-amino-terminated P*i*PrOx (Me-P*i*PrOx-NH_2) allows the synthesis of biocompatible block ionomers based on poly(amino acids) because it can serve as an efficient macroinitiator to allow the ring-opening polymerization of *N*-carboxyanhydrides of protected amino acids (NCA), including ϵ-benzyloxycarbonyl-L-lysine (Lys(Z)-NCA) and β-benzyl-L-aspartate (BLA-NCA).

In this study, we established the novel synthetic route of two kinds of block ionomers composed of P*i*PrOx as a hydrophilic segment with either the oppositely charged poly(amino acid) segment as the other block (P*i*PrOx-P(Lys) or P*i*PrOx-P(Asp)) (Scheme 1). The stable and monodispersive PIC micelles were then prepared through the electrostatic interaction between cationic (P*i*PrOx-P(Lys)) and anionic (P*i*PrOx-P(Asp)) block ionomers in an aqueous medium (Scheme 2) to explore their thermosensitive behavior under physiological conditions using the turbidimetric method. These PIC micelles may offer promising applications as a size-regulated smart nanocontainer loading charged compounds as well as bearing the thermosensitive outer shell that is useful for physical affinity control.

(8) (a) Heskins, M.; Guillent, J. E.; James, E. J. *J. Macromol. Sci. Chem.* **1968**, *A2*, 1441. (b) Schild H. G. *Prog. Polym. Sci.* **1992**, *17*, 163.

(9) (a) Cammas, S.; Suzuki, K.; Sone, Y.; Sakurai, Y.; Kataoka, K.; Okano, T. *J. Controlled Release* **1997**, *48*, 157. (b) Chung, J. E.; Yokoyama, M.; Okano, T. *J. Controlled Release* **2000**, *65*, 93.

(10) (a) Park, J. S.; Akiyama, Y.; Winnik, F. M.; Kataoka, K. *Macromolecules* **2004**, *37*, 6786. (b) Diab, C.; Akiyama, Y.; Kataoka, K.; Winnik, F. M. *Macromolecules* **2004**, *37*, 2556.

Experimental Section

Materials. 2-Isopropyl-2-oxaxoline was synthesized from isobutyric acid (Wako Pure Chemical Industries, Ltd., Japan) and 2-aminoethanol (Wako Pure Chemical) as previously described.[10] Tetrahydrofuran (THF), *n*-hexane, *N*,*N*-dimethylformamide (DMF), and chloroform (Wako Pure Chemical) were purified by distillation following conventional procedures.[11] Trifluoroacetic acid, triethylamine, and acryloyl chloride were purchased from Wako Pure Chemicals and were used without further purification. ϵ-Benzyloxycarbonyl-L-lysine and β-benzyl-L-aspartate were purchased from the Peptide Institute, Inc., Japan, and used without further purification. Bis(trichloromethyl) carbonate (triphosgene) and 30% HBr/AcOH were purchased from Tokyo Kasei Kogyo Co., Ltd., Japan, and used without further purification. The synthesis of two NCAs (ϵ-benzyloxycarbonyl-L-lysine NCA (Lys(Z)-NCA) and β-benzyl-L-aspartate NCA (BLA-NCA)) was carried out by the Fuchs−Farthing method using triphosgene.[12] α-Methyl-ω-amino-poly(2-isopropyl-2-oxazoline) (Me-P*i*PrOx-NH_2, M_n = 4500, M_w/M_n = 1.03, functionality of ω-amino group = ca. 96%) was synthesized as previously described.[10a]

Techniques. The ^{1}H NMR spectra were recorded using a JEOL EX 300 spectrometer at 300 MHz. Chemical shifts were reported in ppm downfield from tetramethylsilane. The molecular weights and molecular weight distributions were determined using a GPC (TOSOH HLC-8220) system equipped with two TSK gel columns ($G4000H_{HR}$ and $G3000H_{HR}$) and an internal refractive index (RI) detector. The columns were eluted with DMF containing lithium bromide (10 mM) at a flow rate of 0.8 mL/min and were maintained at a temperature of 40 °C. The molecular weights were calibrated with poly(ethylene glycol) (PEG) standards (Polymer Laboratories, Ltd., U.K.). The UV−vis spectra were obtained using a V-550 UV/vis Jasco spectrophotometer. Transmission electron microscopy (TEM) was performed using a Hitachi H-7000 operating at an acceleration voltage of 75 kV. Dynamic light scattering (DLS) measurements were carried out using a DLS-7000 instrument (Otsuka Electronics Co., Ltd.). Vertically polarized light at a wavelength of λ_0 = 488 nm from an Ar ion laser was used as the incident beam. The average ζ-potential and light scattering intensity at 90° (SLS mode) were measured using a Zetasizer Nano particle analyzer, NanoZS (green badge, ZEN3500; Malvern, Ltd., Malvern, U.K.) with a green laser (λ = 532 nm).

Synthesis of α-Methyl-ω-acrylate-poly(2-isopropyl-2-oxazoline) (Me-P*i*PrOx-acrylate). For comparison with the thermoresponsive behavior of Me-P*i*PrOx-OH bearing a terminal hydrophilic ω-hydroxyl group, the ω-acrylate-terminated P*i*PrOx (Me-P*i*PrOx-acrylate) was synthesized by the conversion of the ω-hydroxyl group of Me-P*i*PrOx-OH. A 53 mg (0.011 mmol) sample of Me-P*i*PrOx-OH (M_n = 4500, M_w/M_n = 1.03) was dissolved in 0.75 mL of THF with triethylamine (0.0445 g, 0.44 mmol), and acryloyl chloride (0.0195 g, 0.22 mmol) in 0.25 mL of THF was added dropwise to the solution with stirring. The reaction temperature was maintained at 0 °C. After all of the acryloyl chloride was added, the reaction was allowed to continue with stirring for 2 h at 0 °C and for 24 h at room temperature in the dark. The triethylamine hydrochloride salts were then removed by filtration. The resulting solution was dialyzed against methanol and distilled water for 48 h with periodic bath changes to remove any unreacted compounds. The final dialysis product was lyophilized overnight using a freeze dryer to give Me-P*i*PrOx-acrylate (50 mg, ca. 94% yield). The characterization of Me-P*i*PrOx-acrylate was done by MALDI-TOF mass spectrometry (M_n = 4500, M_w/M_n = 1.03, Figure S1 in Supporting Information) and ^{1}H NMR spectroscopy (the conversion efficiency is ca. 80%, Figure S2 in Supporting Information).

Synthesis of Poly(2-isopropyl-2-oxazoline)-*b*-poly(ϵ-benzyloxycarbonyl-L-lysine) Copolymer (P*i*PrOx-P(Lys(Z)) (Run 1 in Table 1). ϵ-Benzyloxycarbonyl-L-lysine NCA (Lys(Z)-NCA; 81 mg, 0.26 mmol) dissolved in 1 mL of DMF was added to a solution of α-methyl-ω-amino-poly(2-isopropyl-2-oxazoline) (Me-P*i*PrOx-NH_2,

(11) Perrin, D. D.; Armarego, W. L. F.; Perrin, D. R. *Purification of Laboratory Chemicals*; Pergamon Press: Oxford, U.K., 1980.

Scheme 2. Schematic Model of the Formation of Thermosensitive Polyion Complex (PIC) Micelles from a Pair of Oppositely Charged Block Ionomers

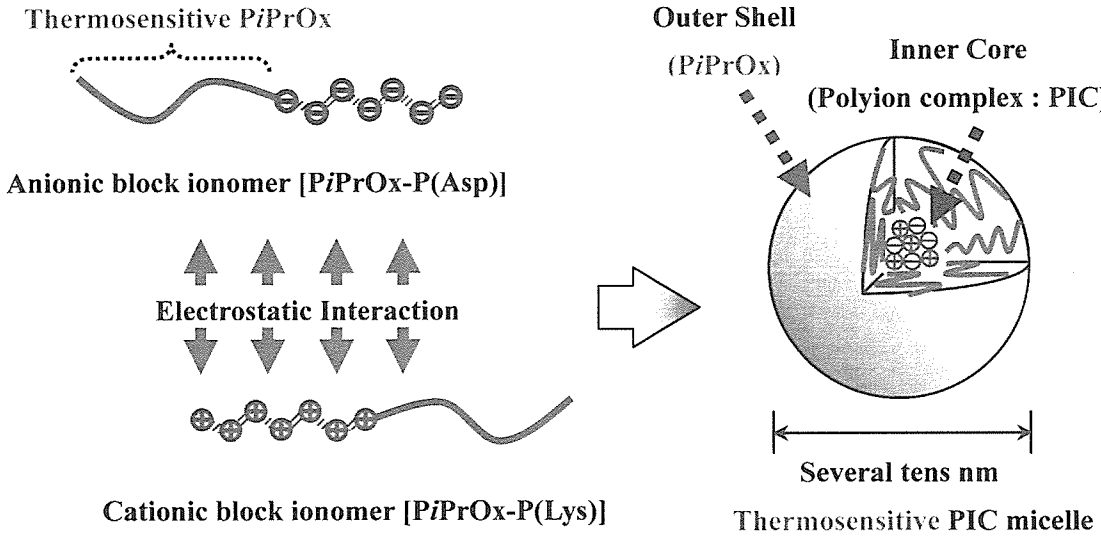

Table 1. Results of Block Copolymer Syntheses (P*i*PrOx-P(Lys(Z)) and P*i*PrOx-PBLA)

P*i*PrOx-P(Lys(Z))[a]								
macroinitiator [MI]			[Lys(Z)-NCA]$_0$				unit ratio[b]	
run	DP[b]	M_w/M_n[b]	[MI]$_0$	time (day)	yield (%)	M($\times 10^{-3}$)[b]	*m*:*n*	M_w/M_n[c]
1	40	1.03	60	4	82	17.6	40:50	1.2
2	40	1.03	80	4	78	21.5	40:79	1.2
P*i*PrOx-PBLA[d]								
macroinitiator [MI]			[BLA-NCA]$_0$				unit ratio[e]	
run	DP[e]	M_w/M_n[e]	[MI]$_0$	time (day)	yield (%)	M_n ($\times 10^{-3}$)[e]	*m*:*n*	M_w/M_n[c]
3	40	1.03	60	3	90	16.2	40:57	1.2
4	40	1.03	80	3	98	20.9	40:80	1.1

[a] Solvent, DMF; [Lys(Z)-NCA]$_0$, 0.1 mmol/mL (run 1), 0.133 mmol/mL (run 2); temp, 37.5 °C. [b] Estimated by ^{1}H NMR in DMSO at 50 °C. [c] Estimated by GPC in DMF containing 10 mM LiCl at 40 °C. [d] Solvent, CH_2Cl_2; [BLA-NCA]$_0$, 0.2 mmol/mL (run 3), 0.267 mmol/mL (run 4); temp, 37.5 °C. [e] Estimated by ^{1}H NMR in DMSO at 50 °C (run 3) and $CDCl_3$ at 25 °C (run 4).

$M_n = 4500$, $M_w/M_n = 1.03$) (20 mg, 0.0044 mmol) in 1 mL of DMF and stirred at 37.5 °C for 4 days under a dry argon atmosphere. The polymerization was monitored by IR spectrometry. After confirming the disappearance of the *N*-carboxyanhydride (NCA) monomers, the mixture was concentrated under reduced pressure and added to 300 mL of *n*-hexane. The precipitate was dissolved in 1 mL of chloroform, followed by reprecipitation into 200 mL of diethyl ether to give P*i*PrOx-P(Lys(Z)) (yield: 82% (83 mg)). The composition of P*i*PrOx-P(Lys(Z)) was determined by GPC and ^{1}H NMR in DMSO-d_6.

Synthesis of Poly(2-isopropyl-2-oxazoline)-*b*-poly(L-lysine) Copolymer (P*i*PrOx-P(Lys)). P*i*PrOx-P(Lys(Z)) (83 mg, 5.4 × 10^{-6} mmol) (run 1 in Table 1) was dissolved in 5 mL of trifluoroacetic acid and stirred for 0.5 h. The solution was then added to 10 mL of a 30 wt % solution of HBr in AcOH, and the reaction mixture was stirred for 2 h at room temperature. Finally, the reaction mixture was precipitated in *n*-hexane, and the product was isolated by repeated precipitations. The product was then redissolved in distilled water and dialyzed against distilled water using a Spectrapor dialysis membrane with a 3500 M_r molecular weight cutoff value. P*i*PrOx-P(Lys) was obtained as a white powder after lyophilization (yield: 78% (65 mg)).

Synthesis of Poly(2-isopropyl-2-oxazoline)-*b*-poly(aspartic acid) Copolymer (P*i*PrOx-P(Asp)). β-Benzyl-L-aspartate NCA (BLA-NCA; 66 mg, 0.26 mmol) dissolved in 1 mL of dichloromethane was added to a solution of α-methyl-ω-amino-poly(2-isopropyl-2-oxazoline) (Me-P*i*PrOx-NH_2, $M_n = 4500$, $M_w/M_n = 1.03$) (20 mg, 0.0044 mmol) in 1 mL of dichloromethane and stirred at 37.5 °C for 3 days under a dry argon atmosphere. A procedure similar to that for P*i*PrOx-P(Lys(Z)) was also adapted for P*i*PrOx-PBLA (run 3 in Table 1). P*i*PrOx-P(Asp) was then prepared from P*i*PrOx-PBLA by the removal of the benzyl groups in 0.5 N NaOH at room temperature (reaction time 5 h). (yield: 95% (55 mg)).

Preparation of Polyion Complex Micelles. P*i*PrOx-P(Lys) and P*i*PrOx-P(Asp) were separately dissolved in a Tris-HCl buffered solution (10 mM, pH 7.4) with or without a varying NaCl concentration of 10, 100, and 150 mM, respectively. After filtration through a 0.4 μm filter (MILLEX-VV, Millipore), the polyion complex micelles were prepared by mixing these solutions in an equal unit ratio of L-lysine and aspartic acid residues in the block copolymers (total concentration: 1.0 mg/mL).

Dynamic Light Scattering (DLS) Measurements. All samples were stored overnight before the measurements and used without further purification. All measurements were performed at 20 °C. Details of the data analysis procedure have been described eleswhere.[4a,13]

Transmission Electron Microscopy (TEM). For the observation of the size and distribution of the micellar particles, a drop of the sample solution (concentration = 0.125 mg/mL) was placed onto a 400 mesh copper grid coated with a 0.5 wt % poly(vinyl formal) aqueous solution. About 2 min after deposition, the grid was touched with filter paper to remove the surface water, followed by air drying. Negative staining was performed using a droplet of a 1 wt % uranyl acetate solution. The samples were air dried before the measurement.

(12) (a) Daly, H. W.; Poche, D. *Tetrahedron Lett.* **1988**, *29*, 5859. (b) Fasman, G. D.; Idelson, M.; Blout, E. R. *J. Am. Chem. Soc.* **1961**, *83*, 709.

(13) (a) Xu, R.; Winnik, M. A.; Hallett, F. R.; Riess, G.; Croucher, M. D. *Macromolecules* **1991**, *24*, 87. (b) Harada, A.; Kataoka, K. *Macromolecules* **1998**, *31*, 288.

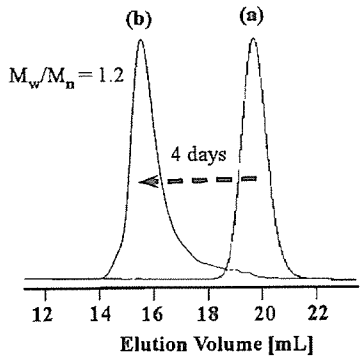

Figure 1. Gel permeation chromatograms of (a) Me-P*i*PrOx-NH_2 and (b) P*i*PrOx-P(Lys(Z)) (PEG standard; eluant, DMF (containing 10 mM LiCl); temperature, 40 °C; RI detection).

Turbidity Measurements Using the UV−Vis Spectrophotometer. The cloud points (T_{cp}) were determined by the spectrophotometric detection of the changes in the transmittance ($\lambda = 500$ nm) of the aqueous polymer solutions heated at a constant rate (0.5 °C min^{-1}). The samples were thermostated using a temperature-controlled circulating water bath. Cloud-point values of the polymer solutions were determined as the temperature corresponding to a 10% decrease in the optical transmittance.

Results and Discussion

Synthesis of Block Copolymers. In this study, ω-amino-terminated poly(2-isopropyl-2-oxazoline) (Me-P*i*PrOx-NH_2) (M_n = 4500, M_w/M_n = 1.03) was employed as a macroinitiator for the anionic ring-opening polymerization of NCA to form the block copolymers of P*i*PrOx and protected poly(amino acid) (P*i*PrOx-P(Lys(Z)) or P*i*PrOx-PBLA). The synthesized block copolymers were characterized by GPC and ^{1}H NMR as summarized in Table 1. Figure 1 shows the GPC profiles of the macroinitiator (Me-P*i*PrOx-NH_2) and the block copolymer (P*i*PrOx-P(Lys(Z))). After block copolymerization was carried out for 4 days, the peak shifted to a smaller elution volume because of an increase in the molecular weight. No peak of the macroinitiator remained, indicating the high efficiency of the block copolymerization. Figure 2 shows the ^{1}H NMR spectra of the block copolymer before (Figure 2a) and after (Figure 2b) the deprotection of the ϵ-benzyloxycarbonyl groups under the acidic conditions (30% HBr/AcOH) for run 1 in Table 1. Comparing the peak integral ratio of the methyl protons of P*i*PrOx ($(CH_3)_2$: δ 1.0) and the methylene protons of the ϵ-benzyloxycarbonyl group of P(Lys(Z)) ($CH_2C_6H_5$: δ 4.9), the DP of Lys(Z) was calculated to be 50. For P*i*PrOx-P(Lys) in Figure 2b, the peak integral ratio of the methyl protons of P*i*PrOx ($(CH_3)_2$: δ 1.0) and α-methine protons of P(Lys) (CO*CH*NH: δ 4.2) was measured in order to calculate the DP that was determined to be 52. It was confirmed from the similar DP values of lysine units for P*i*PrOx-P(Lys(Z)) and P*i*PrOx-P(Lys) that neither the loss of the lysine repeating units by backbone scission nor cleavage of the amide group to a secondary amino group in the side chain of the P*i*PrOx block occurred during the deprotection reaction. On the basis of these results, it was ascertained that the polymerization of Lys(Z)-NCA was successfully accomplished using the ω-amino-terminated P*i*PrOx macroinitiator: the polydispersity indices were about 1.2, and the experimental value of the degree of polymerization (DP) was close to the value predicted from the initial monomer/macroinitiator ratio (60/1). The P*i*PrOx-P(Lys) block ionomers (P*i*PrOx; M_n = 4500 g/mol) with different DP values of the P(Lys) segments, 52 and 82, are abbreviated 45C52 and 45C82, respectively.

In a similar fashion, the synthesis of P*i*PrOx-PBLA was performed as shown in Table 1 (runs 3 and 4). From the GPC

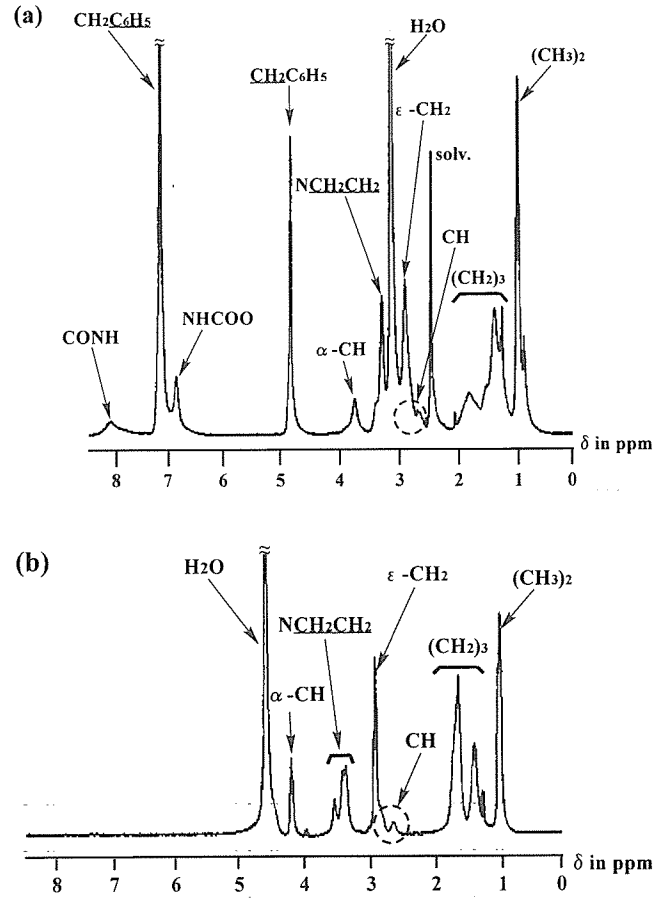

Figure 2. ^{1}H NMR spectra of (a) P*i*PrOx-P(Lys(Z)) in DMSO-d_6 at 50 °C and (b) P*i*PrOx-P(Lys) in D_2O at 20 °C.

of the obtained P*i*PrOx-PBLA (run 3 in Table 1, Figure S3 in Supporting Information), a unimodal peak was also observed in the reaction mixture after 3 days as in the case of P*i*PrOx-P(Lys-(Z)). To assign the composition of P*i*PrOx-PBLA, the ^{1}H NMR was measured in DMSO-d_6 (run 3) (Figure S4 in Supporting Information). From the peak integral ratio of the methyl protons of P*i*PrOx ($(CH_3)_2$: δ 1.0) to the benzyl protons of PBLA ($COOCH_2C_6H_5$: δ 7.2), the DP of BLA was determined to be 57. The ^{1}H NMR spectrum of P*i*PrOx-P(Asp) in D_2O, obtained after deprotection of the benzyl groups of P*i*PrOx-PBLA (run 3), is also shown in Figure S5 of Supporting Information. Although some of the peaks assigned to the methylene protons of the α,β linkages of P(Asp) (δ 2.7)[14] were superposed on a broad peak assigned to the methine proton of the isopropyl group of P*i*PrOx (δ 2.4−2.9), the DP (53) calculated from the integral ratio of the methyl protons of P*i*PrOx ($(CH_3)_2$: δ 1.0) to the methylene protons of the α,β linkages of P(Asp) (δ 2.7) was also in a good agreement with the result (DP = 57) for P*i*PrOx-PBLA. The P*i*PrOx-P(Asp) block ionomers (P*i*PrOx; M_n = 4500 g/mol) with different DP values of the P(Asp) segments, 53 and 76, are abbreviated 45A53 and 45A76, respectively.

Preparation of Polyion Complex Micelles. The PIC micelles were formed by mixing 1.0 mg/mL Tris-HCl solutions of P*i*PrOx-P(Lys) and P*i*PrOx-P(Asp) under stoichiometric conditions in which the unit ratio of the L-lysine in P*i*PrOx-P(Lys) and aspartate in P*i*PrOx-P(Asp) was unity. This procedure of PIC micelle formation by the simple mixing of a pair of oppositely charged

(14) (a) Yokoyama, M.; Miyauchi, M.; Yamada, N.; Okano, T.; Sakurai, Y.; Kataoka, K.; Inoue, S. *J. Controlled Release* **1990,** *11,* 269. (b) Yokoyama, M.; Inoue, S.; Kataoka, K.; Yui, N.; Okano, T.; Sakurai, Y. *Makromol. Chem.* **1989,** *190,* 2041.

Table 2. Size and Polydispersity Index Values of the PIC Micelles

samples	concentration (mg/mL)	D_T[a] (10^{-7}cm^2/s)	μ_2/Γ^2[a]	R_h[b] (nm)	diameter (nm) mean cumulative[a]	diameter (nm) z-weighted[c]	d_w/d_n[c]
45C52/45A53	1	1.306	0.078		36.2	37.0 ± 8.4	1.16
	0.5	1.237	0.062	18.0	36.6	38.8 ± 7.7	1.15
	0.25	1.218	0.121		37.2	41.2 ± 13.1	1.21
	0.125	1.208	0.178		37.7	41.3 ± 16.2	1.19
45C82/45A76	1	0.819	0.044		39.6	41.0 ± 8.7	1.11
	0.5	0.833	0.075	22.6	39.5	42.6 ± 12.0	1.17
	0.25	0.823	0.059		40.0	42.6 ± 12.9	1.17
	0.125	0.822	0.044		40.1	41.8 ± 9.9	1.13

45C52/45A53 (1 mg/mL)	D_T[a] (10^{-7}cm^2/s)	μ_2/Γ^2[a]	diameter (nm) mean cumulative[a]	diameter (nm) z-weighted[c]	d_w/d_n[c]
10 mM NaCl	1.134	0.069	32.6	34.9 ± 9.1	1.15
100 mM NaCl	1.107	0.065	33.2	35.8 ± 9.3	1.16
150 mM NaCl	1.048	0.094	36.6	37.6 ± 8.8	1.13

[a] Obtained by cumulant analysis of dynamic light scattering (DLS). [b] Determined from the diffusion coefficient at infinite dilution (D_0) using the Stokes–Einstein equation. [c] Calculated by the histogram method. (d_w and d_n denote the weight- and number-average diameters, respectively.)

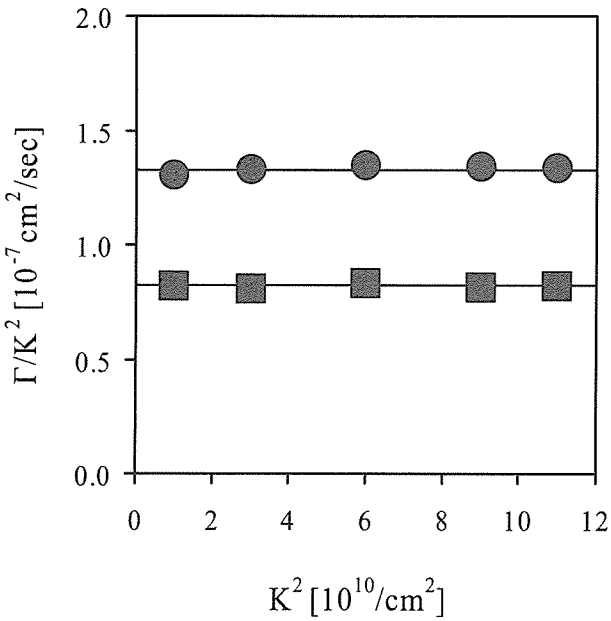

Figure 3. Relationship between the scaled average characteristic line width (Γ/K^2) and the magnitude of the scattering vector (K^2) for PIC micelles (45C52/45A53, ●; 45C82/45A76, ■; total concentration, 1.0 mg/mL; temperature, 20 °C; detection angles, 30, 60, 90, 120, and 150°; solvent, 10 mM Tris-HCl).

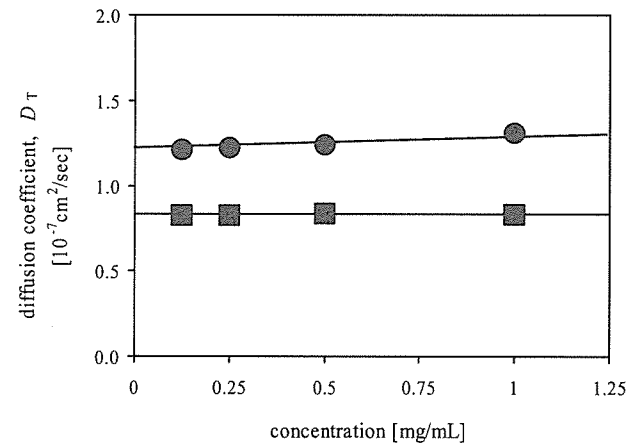

Figure 4. Plots of the translational diffusion coefficient (D_T) vs the total concentration of PIC micelles (45C52/45A53, ●; 45C82/45A76, ■; (temperature, 20 °C; detection angle, 90°; solvent, 10 mM Tris-HCl).

block ionomers had previously been established by our group for the PEG-P(Lys) and PEG-P(Asp) pair.[5a] The prepared solution was stored overnight in the refrigerator before DLS characterization.

Two pairs of PIC micelles were prepared by mixing the P*i*PrOx-based block ionomers with different charge lengths (Table 2): one comprising 45C52 where the unit number of L-lysine is 52 and 45A53 with the unit number of aspartate of 53 and the other comprising 45C82 where the unit number of L-lysine is 82 and 45A76 with the unit number of aspartate of 76. To investigate the shape as well as the size of the PIC micelles, angle-trace DLS measurements were carried out at 30, 60, 90, 120, and 150° detection angles at 20 °C. The sufficiently low temperature condition (20 °C) had to be adapted for all of the sample measurements, excluding the unexpected change in the shape or size of the PIC micelles, possibly derived from the collapse of the P*i*PrOx segments around the phase-transition temperature. Figure 3 shows the relationship between the scaled average of the scattering characteristic line width (Γ/K^2) and the magnitude of the scattering vector (K^2) at a concentration of 1 mg/mL. The Γ/K^2 values of the PIC micelles formed between P*i*PrOx-P(Lys) and P*i*PrOx-P(Asp) were independent of the detection angle in all cases. These results agreed with the fact that the Γ/K^2 values should be independent of the detection angle in the case of spherical particles. Because the angular dependence of Γ/K^2 was almost negligible, the following DLS measurements were performed at a 90° detection angle.

Figure 4 shows the concentration dependence of the diffusion coefficient (D_T). The PIC micelles were prepared by mixing the solutions of P*i*PrOx-P(Lys) and P*i*PrOx-P(Asp) (45C52/45A53 and 45C82/45A76 in Table 2) with diluting concentrations from 1 to 0.125 mg/mL under an electrostatically neutralized condition (1:1 unit ratio of L-lysine and aspartate residues). It is obvious that the diffusion coefficients were almost independent of the concentrations of both 45C52/45A53 and 45C82/45A76, indicating that the change in the total concentration induces no formation of secondary aggregates. It is likely that the P*i*PrOx shell layer may prevent the clustering of the micelles due to a steric repulsion mechanism, which is consistent with the formation of a core–shell structure. The diffusion coefficient at infinite dilution D_0 was then determined to be 1.187×10^{-7} cm^2/s (from 45C52/45A53 in Table 2) and 0.822×10^{-7} cm^2/s (from 45C82/45A76 in Table 2), respectively, for the 45C52/45A53 and 45C82/45A76

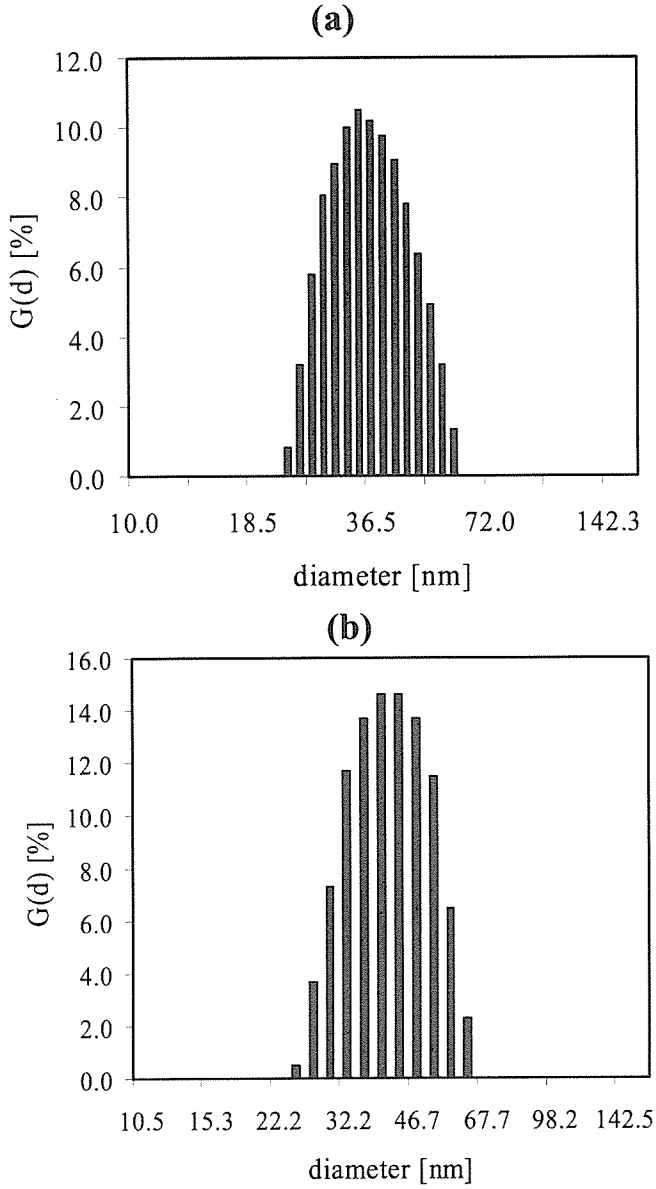

Figure 5. Γ-averaged size distribution analyzed by the histogram method for PIC micelles: (a) 45C52/45A53 and (b) 45C82/45A76 (total concentration, 1.0 mg/mL; temperature, 20 °C; detection angle, 90°; solvent, 10 mM Tris-HCl).

systems. From the obtained D_0 value, values of the hydrodynamic radius (R_h) were calculated to be 18.0 and 22.6 nm using the Stokes–Einstein equation. Obviously, the R_h values slightly increased with an increase in the length of the charged segments. The polydispersity indices (μ_2/Γ^2) (Table 2) were small enough to consider that the micelles have a narrow size distribution. This narrow size distribution is in good agreement with the result of the independence of the Γ/K^2 value versus the detection angle, as shown in Figure 3.

Figure 5 shows the Γ-averaged size distribution of the polyion complex micelles (1 mg/mL) obtained from the histogram analysis of the DLS data at 20 °C. It was confirmed from the size distribution profiles that the micelles prepared were unimodal with average diameters of 37.0 ± 8.4 and 41.0 ± 8.7 nm, respectively (Figure 5a and b for the 45C52/45A53 and 45C82/45A76 systems). These were in good agreement with the mean cumulative diameters (36.2 and 39.6 nm) and R_h values (18.0 and 22.6 nm) calculated from the cumulant analysis. All of the data including the polydispersity index (d_w/d_n) values obtained from this histogram method are also summarized in Table 2.

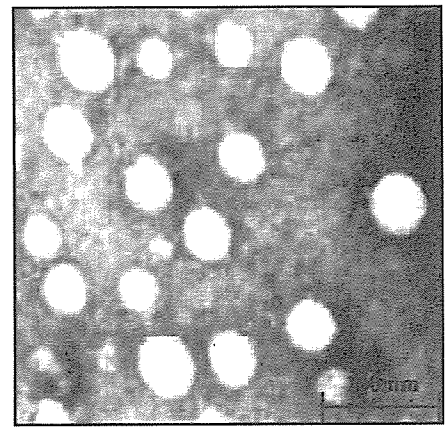

Figure 6. TEM image of PIC micelles formed from 45C52 and 45A53 in distilled water at room temperature (concentration, 0.125 mg/mL; negative staining by a 1 wt % uranyl acetate solution).

Furthermore, it was confirmed that monodisperse spherical particles with an ~40 nm diameter were clearly observed in the TEM image of the PIC micelles from 45C52/45A53 prepared in distilled water (Figure 6).

The electrophoretic mobility of the PIC micelle (45C52/45A53) was also determined to be −0.04745 ± 0.0105 μm cm/Vs on the basis of laser-Doppler electrophoresis. The average ζ-potential was then calculated from this value using the Smoluchowski equation.[5a] The calculated average ζ-potential of the PIC micelles had an extremely small absolute value (−0.6690 ± 0.148 mV), indicating the shielding of the PIC core by the electrically neutral shell of the P*i*PrOx segments.

On the basis of the results of the DLS, TEM, and ζ-potential described above, it is reasonable to conclude that the micelles having the PIC core were surrounded by P*i*PrOx as the shell layer and were stably dispersed with a narrow, unimodal distribution in an aqueous entity at 20 °C. It is known that the stability of the polyion complex is strongly affected by the ionic strength of the medium (i.e., destabilized with an increase in the ionic strength due to electrostatic shielding[15]). The effect of the ionic strength on the stability of the PIC micelles was estimated by measuring the size of the PIC micelle solutions (1 mg/mL) under several NaCl concentrations. The diffusion coefficients (D_T) remained constant almost up to the 150 mM NaCl concentration value, viz., near physiological conditions, meaning that the stability of the PIC micelles is sufficient under the measured ionic strengths (Table 2 and Figure 7a–c).

Determination of the Cloud Points (T_{cp}). As the first step in our study of the thermoresponsive behavior of the P*i*PrOx-based PIC micelles, we examined in detail the cloud-point (T_{cp}) values of the P*i*PrOx oligomer solutions. It was necessary to select two parameters, such as the oligomer and NaCl concentrations, when considering the future application of the PIC micelles under physiological conditions. In addition, ω-acrylate-terminated P*i*PrOx (Me-P*i*PrOx-acrylate) was prepared by end capping the ω-hydroxyl group of Me-P*i*PrOx-OH in order to explore the effects of the terminal end groups on T_{cp}, which are presumably pronounced for the oligomer solutions.

The open (in the absence of NaCl) and closed (in the presence of 150 mM NaCl) symbols in Figures 8a and b show the turbidity changes in the aqueous solutions of Me-P*i*PrOx-OH (M_n = 4500, M_w/M_n = 1.03) (square symbols) and Me-P*i*PrOx-acrylate (M_n = 4500, M_w/M_n = 1.03) (circle symbols) bearing the same chain length as that used in the synthesis of the block ionomers under

(15) (a) Abe, K.; Ohno, H.; Tsuchida, E. *Makromol. Chem.* **1977**, *178*, 2285. (b) Tsuchida, E.; Osada, Y.; Ohno, H. *J. Macromol. Sci. Phys.* **1980**, *B17*, 683.

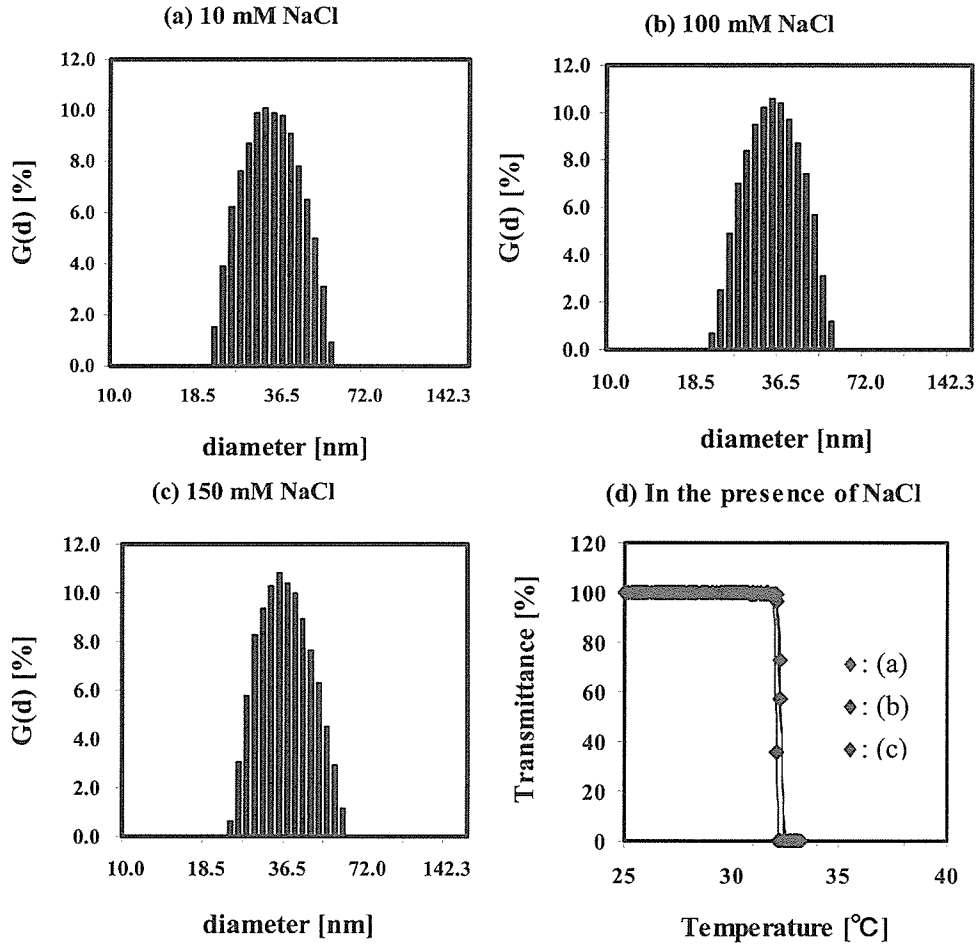

Figure 7. Γ-averaged size distribution analyzed by the histogram method for 45C52/45A53 with different NaCl concentrations: (a) 10, (b) 100, and (c) 150 mM. (d) Respective transmittance changes at 500 nm as a function of temperature (total concentration, 1.0 mg/mL; temperature, 20 °C; detection angle, 90°; solvent, 10 mM Tris-HCl; rate, 0.5 °C/min).

several concentrations (1−10 mg/mL). The T_{cp} values of Me-P*i*PrOx-acrylate, dissolved in 10 mM Tris-HCl buffer (pH 7.4), exhibited a remarkable dependence on the concentrations of both the oligomer and NaCl. The transmittance curves become duller by shifting to a higher temperature region as a result of the decreasing concentration of the oligomer solutions. Obviously, more than a 5 °C decrease in T_{cp} was observed at every oligomer concentration by adding 150 mM NaCl to the solution (Figures 8 and 9) Also, there was a gradual decrease in the T_{cp} at each oligomer concentration with an increase in the NaCl concentration (10, 100, 150 mM) (Figure 9) Alternatively, all of the ω-hydroxyl-terminated P*i*PrOx oligomers (Me-P*i*PrOx-OH) exhibited a sharp thermoresponsivity in the relatively higher temperature region (44−51 °C) compared to that of the Me-P*i*PrOx-acrylate, and the dependency of T_{cp} on the oligomer and NaCl concentrations was less pronounced. As the NaCl concentration increased from 0 to 150 mM, the decrease in the T_{cp} of Me-P*i*PrOx-OH was only in the range of a few degrees (Figures 8 and 9).

Note that turbidimetric behavior similar to that of P*i*PrOx has also been observed for poly(*N*-isopropylacrylamide) (PNIPAAm), a typical thermosensitive polymer as well as the chemical isomer of P*i*PrOx, at least in a similar molecular weight ($M_n \leq$ ca. 10 000) range. In particular, the LCST values of the end-functionalized PNIPAAm oligomers ($M_n \leq$ ca. 10 000) were found to have a significant dependence on either the hydrophilic or hydrophobic property of the terminal end group. For instance, ω-hydroxyl-terminated PNIPAAm with lower molecular weight from 3300 to 8000 demonstrated even higher LCST values of ca. 36−50 °C.[16b,c] This was considered to be a result of the comparatively enhanced hydrating contribution of hydrophilic ω-hydroxyl groups in the PNIPAAm oligomers, compared to that for those of higher molecular weight in which the ratio of the ω-terminal hydroxyl groups to the backbone is lower. In contrast, PNIPAAm with hydrophobic terminal ends, such as alkyl, phenyl, and pyrenyl groups, had LCST values shifted toward lower temperatures, which were quite pronounced with decreasing molecular weight.[16a,b,d−g] Moreover, the PNIPAAm oligomers with hydrophilic terminal ends showed relatively sharp transitions, whereas those of the hydrophobic terminal ends had a tendency toward early onset as well as also decreasing in their cloud-point curves, presumably resulting from the difference in the rate of aggregation.[16g] On the basis of these results from the PNIPAAm oligomer solutions, a similar explanation could be adapted for the higher T_{cp} values exhibiting a sharper transition of Me-P*i*PrOx-OH with the hydrophilic ω-hydroxyl groups than those of Me-P*i*PrOx-acrylate with hydrophobic ω-acrylate groups. As far as the notable dependency of T_{cp} of the P*i*PrOx oligomers on the NaCl concentration, this could be understood through the well-known "salting-out" effect of NaCl,[17] as also observed in previous studies of polyoxazolines including P*i*PrOx.[18] The T_{cp} values of

(16) (a) Chung, J. E.; Yokoyama, M.; Suzuki, K.; Aoyagi, T.; Sakurai, Y.; Okano, T. *Colloids Surf., B* **1997**, *9*, 37. (b) Chung, J. E.; Yokoyama, M.; Aoyagi, T.; Sakurai, Y.; Okano, T. *J. Controlled Release* **1998**, *53*, 119. (c) Kohori, F.; Sakai, K.; Aoyagi, T.; Yokoyama, M.; Sakurai, Y.; Okano, T. *J. Controlled Release* **1998**, *55*, 87. (d) Xia, Y.; Yin, X.; Burke, N. A. D.; Stöver, H. D. H. *Macromolecules* **2005**, *38*, 5937. (e) Duan, Q.; Miura, Y.; Narumi, A.; Shen, X.; Sato, S.-I.; Satoh, T.; Kakuchi, T. *J. Polym. Sci., Part A: Polym. Chem.* **2006**, *44*, 1117. (f) Furyk, S.; Zhang, Y.; Ortiz-Acosta, D.; Cremer, P. S.; Bergbreiter, D. E. *J. Polym. Sci., Part A: Polym. Chem.* **2006**, *44*, 1492. (g) Xia, Y.; Burke, N. A. D.; Stöver, H. D. H. *Macromolecules* **2006**, *39*, 2275.

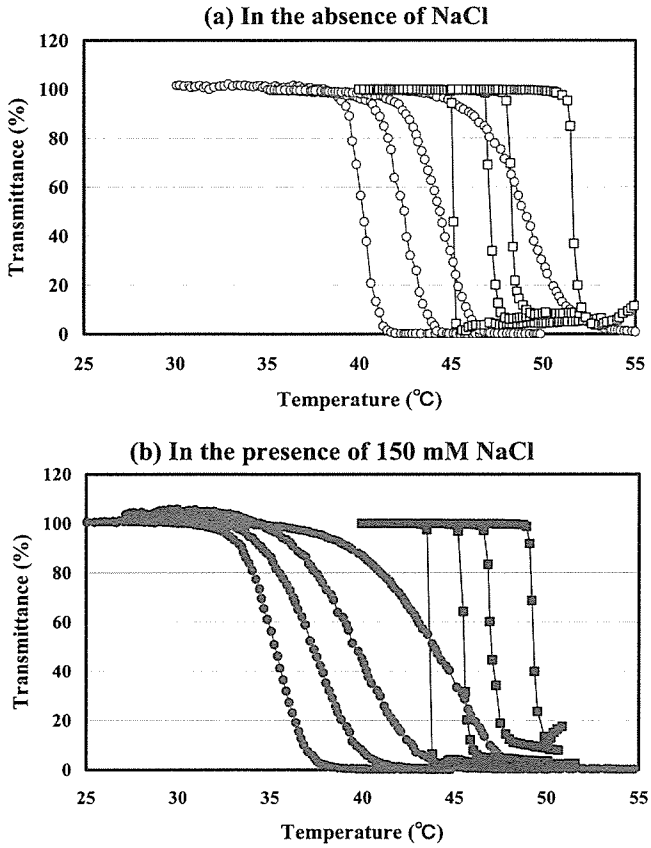

Figure 8. Transmittance changes at 500 nm as a function of temperature under different oligomer concentrations (1−10 mg/mL): (a) in the absence of NaCl (Me-P*i*PrOx-acrylate, $M_n = 4500$, $M_w/M_n = 1.03$; open circle), Me-P*i*PrOx-OH ($M_n = 4500$, $M_w/M_n = 1.03$; open square) and (b) in the presence of 150 mM NaCl (Me-P*i*PrOx-acrylate, solid circle; Me-P*i*PrOx-OH, solid square); 10 mM Tris-HCl buffered solution (pH 7.4); rate, 0.5 °C/min).

the respective P*i*PrOx oligomer solutions decrease with increasing concentration of NaCl up to 150 mM. In particular, the NaCl concentration effect on the decreasing T_{cp} values of Me-P*i*PrOx-OH was relatively alleviated compared to that of the Me-P*i*PrOx-acrylate, as a result of the existence of a hydrophilic hydroxyl group at the ω-terminal end (Figures 8 and 9). In other words, it was obvious that the salting-out effect of NaCl to decrease the affinity or solubility power of water against the hydrophilic carbonyl groups at the side chain of the Me-P*i*PrOx-OH oligomer solutions was reduced by the strong hydrating contribution of the terminal ω-hydroxyl groups.

Interestingly, the T_{cp} value of neither the 45C52 nor the 45A53 block ionomer solution both in the absence and the presence of 150 mM NaCl was detected in the measured temperature range up to 75 °C, suggesting the strong hydrating effect of the ionized groups at the side chains of a charged block segment of ionomers (Figure 10a and b). Although there is also possibility for the block ionomer systems to form nanometer-scale micelles composed of a hydrophilic charged outer shell and a hydrophobic P*i*PrOx inner core resulting from aggregation among the P*i*PrOx oligomers collapsed over the phase-separation temperature, it was ascertained from the static light scattering (SLS) measurement that no evidence of micellar formation, such as an increase in the light scattering intensity, was observed for the respective

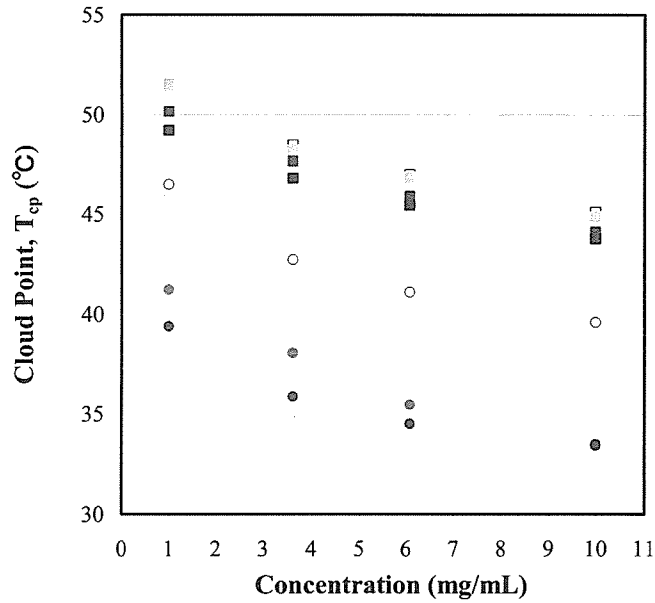

Figure 9. Plots of the changes in the cloud point (T_{cp}) determined from Figure 8 as a function of the respective oligomer concentration (1−10 mg/mL) (Me-P*i*PrOx-acrylate with 0, open circle; 10, solid light-green dot; 100, dark-green solid dot; and 150 mM NaCl, solid blue dot; Me-P*i*PrOx-OH with 0, open square; 10, light-orange solid square; 100, medium-orange solid square; and 150 mM NaCl, red solid square).

ionomer solutions in the measured temperature range (25−75 °C) (data not shown).

We next investigated the thermoresponsive behavior of P*i*PrOx under the formation of PIC micelles. Figure 10a also shows the transmittance changes in the 45C52/45A53 PIC micelles under several total concentrations (0.125, 0.25, 0.5, and 1 mg/mL; 10 mM Tris-HCl buffered solution (pH 7.4) in the absence of NaCl). The results showed a unique characteristic of the PIC micelles. Indeed, the T_{cp} values for the PIC micelles were observed to shift remarkably to a lower temperature than for the P*i*PrOx oligomers (Me-P*i*PrOx-OH and Me-P*i*PrOx-acrylate). Furthermore, all of the micelles with different total concentrations underwent an agglomeration even at a same constant temperature of ca. 33 °C. It was already confirmed in Table 2 and Figure 4 that the diffusion coefficients (D_T) and hence the cumulative average diameters of the PIC micelles remained almost constant under the wide concentration conditions down to 0.125 mg/mL at 20 °C, indicating that the micelles stably exist in the measured concentration region (0.125−1 mg/mL). In addition, the transmittance changes at a constant total concentration (1 mg/mL) but containing different NaCl concentrations up to 150 mM, as was also observed as shown in Figure 7d. The T_{cp} values of the PIC micelles coexisting with NaCl also exhibited a similar temperature, ca. 32 °C, which is similar to that in the absence of NaCl regardless of the NaCl concentration up to 150 mM. Moreover, the turbidimetric behavior of the 45C52/45A53 micelles in the presence of 150 mM NaCl was also investigated by diluting the total concentration from 1 to 0.125 mg/mL (Figure 10b). All of the micelles also showed a turbidity near the constant temperature of ca. 32 °C, and the changing behavior of the transmittance curves was similar to that in Figure 10a. Concerning the 45C52/45A53 micelles under 0.125 mg/mL, it was notable that the turbidimetric curve was rather broadly decreasing with increasing temperature compared to the initial sharp responsivity, obviously resulting from the dependence on the rate of temperature increase (Figure S6 in Supporting Information).

(17) (a) Eeckman, F.; Amighi, K.; Moës, A. J. *Int. J. Pharm.* **2001**, *222*, 259. (b) Freitag, R.; Garret-Flaudy, F. *Langmuir* **2002**, *18*, 3434. (c) Liu, X. M.; Wang, L. S.; Wang, L.; Huang, J.; He, C. *Biomaterials* **2004**, *25*, 5659.

(18) (a) Lin, P.; Pearce, E. M.; Kwei, T. K. *J. Polym. Sci., Part B: Polym. Phys.* **1988**, *26*, 603. (b) Uyama, H.; Kobayashi, S. *Chem. Lett.* **1992**, 1643.

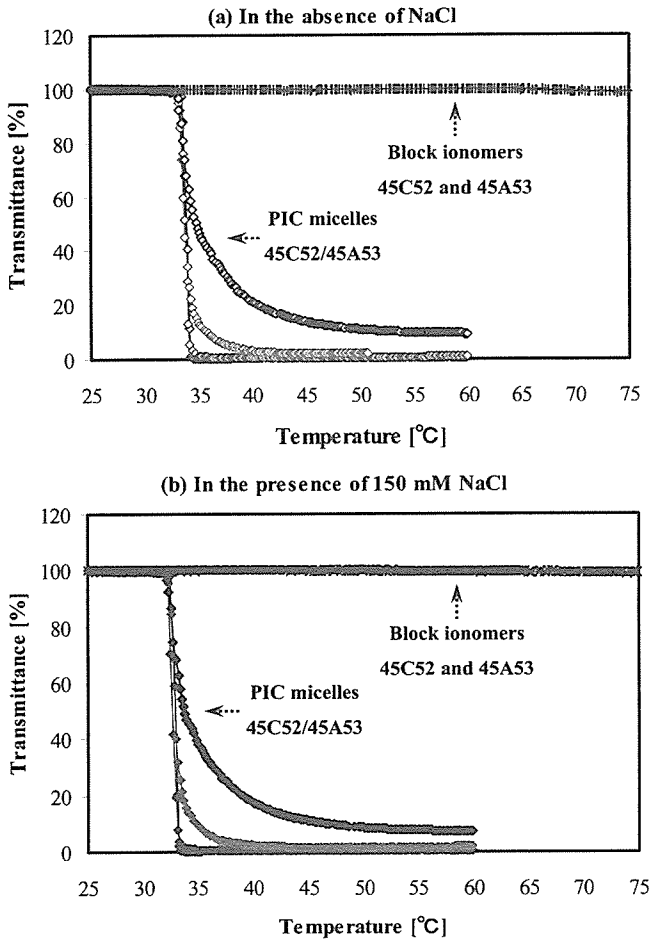

Figure 10. Transmittance changes at 500 nm as a function of temperature for oppositely charged block ionomers (45C52 and 45A53) and their PIC micelles (45C52/45A53): (a) in the absence of NaCl: block ionomers, +; PIC micelles (◇, 0.125 mg/mL; open green diamond, 0.25 mg/mL; open blue diamond, 0.5 mg/mL; and open red diamond, 1 mg/mL) and (b) in the presence of 150 mM NaCl: block ionomers, ×; PIC micelles (◆, 0.125 mg/mL; solid green diamond, 0.25 mg/mL; solid blue diamond, 0.5 mg/mL; and open red diamond, 1 mg/mL); 10 mM Tris-HCl buffered solution (pH 7.4); rate, 0.5 °C/min.

It should be noted that the T_{cp} values for the PIC micelles significantly shifted to a lower temperature (ca. 32−33 °C) when comparing two end-functionalized P*i*PrOx oligomers (Me-P*i*PrOx-OH and Me-P*i*PrOx-acrylate) and, in addition, were almost constant regardless of the total concentration of the system with or without NaCl (≤150 mM). It is reasonable to suggest that the remarkable decrease in T_{cp} may be related to the high local concentration of the P*i*PrOx segments on micelles with an appreciable increase in the apparent molecular weight. To put it more concretely, whereas the P*i*PrOx oligomer solutions were significantly related to the intermolecular aggregation behavior through the notable concentration-dependent dehydration process with increasing temperature, the supramolecular assembly, such as PIC micelles with densely packed outer shells, may prefer rapid intramicellar aggregation with an accelerated dehydration process resulting from the high local concentration of the micelles' shell layer. As a result, the T_{cp} values for the PIC micelles could be appreciably shifted to a lower temperature (ca. 32 °C) even rarely depending on the total concentration including NaCl up to 150 mM. In addition, another possible factor is also considered to be the effect of terminal end groups. The ω terminal groups of the P*i*PrOx oligomers, fixed on the shell surface of the present PIC micelles, could not be expected to interfere with the shifts in T_{cp}. However, it seemed that the hydrophobic methyl groups at the α-terminal ends of the P*i*PrOx oligomers, accumulated on the outermost micelle surfaces through self-assemblies among block ionomers, were also connected with the decreasing T_{cp} of the PIC micelles. As appreciated from the fact that the T_{cp} of Me-P*i*PrOx-acrylate with hydrophobic groups at both terminal ends decreased at a high rate with increasing concentration when comparing Me-P*i*PrOx-OH with the hydrophilic ω-hydroxyl ends, the T_{cp} of PIC micelles could be affected by the hydrophobic methyl groups existing on the outermost micelles surfaces. A similar result is that the presence of the hydrophilic or hydrophobic groups on the outermost surface of the polymeric micelles strongly influenced the shift in the LCST values of the micelles, which was also observed in the micelle system composed of the thermosensitive PNIPAAm outer shell and hydrophobic inner core.[19] Considering the future application as thermosensitive drug delivery vehicles, such as responding to local hyperthermia, it was highly desirable that the T_{cp} of the thermosensitive PIC micelles should be constant regardless of the wide concentration range under physiological conditions. Moreover, the present PIC micelles might be dissociated into free block ionomers not showing thermosensitivity under specific conditions, suggesting their facile separation after fulfilling their mission as a thermosensitive vehicle.

Conclusions

The controlled synthesis of oppositely charged block ionomers (P*i*PrOx-P(Lys) and P*i*PrOx-P(Asp)) was achieved via ring-opening anionic polymerization of *N*-carboxyanhydrides (NCA) (ϵ-benzyloxycarbonyl-L-lysine (Lys(Z)-NCA) and β-benzyl-L-aspartate (BLA-NCA)) with ω-amino-functionalized P*i*PrOx macroinitiators and the subsequent deprotection reaction. Then, polyion complex (PIC) micelles were prepared by the complexation of P*i*PrOx-P(Lys) and P*i*PrOx-P(Asp) under physiological conditions. It was confirmed that the PIC micelles were spherical particles with small polydispersity indices and were very stable without any secondary aggregates. Furthermore, these PIC micelles had a constant phase-separation temperature (ca. 32 °C) under physiological conditions regardless of the wide ranges of concentration, reflecting the increased local concentration of the P*i*PrOx segments in the shell layer. In this respect, the P*i*PrOx-based PIC micelles might have promising applications, especially as a thermosensitive drug carrier loading charged biomacromolecules that include proteins, nucleic acids, and enzymes.

Acknowledgment. This work was financially supported by Special Coordination Funds for Science and Technology from the Ministry of Education, Culture, Sports, Science and Technology of Japan (MEXT) and by the Core Research for Evolution of Science and Technology (CREST), Japan Science and Technology Corporation (JST). We express our appreciation to Professor Woo-Dong Jang, The University of Tokyo (Present address: Yonsei University, Korea) and Mr. Shigeto Fukushima, Nippon Kayaku Co., Ltd., Japan, for their help with the NCA synthesis and Ph.D. candidate Michiaki Kumagai, The University of Tokyo, for his support with the acquisition of the TEM image.

Supporting Information Available: MALDI-TOF mass spectrum of Me-P*i*PrOx-acrylate obtained after the conversion reaction. ^{1}H NMR spectra of Me-P*i*PrOx-acrylate in D_2O, Me-P*i*PrOx-PBLA in DMSO-d_6, and P*i*PrOx-P(Asp) in D_2O. Gel permeation chromatograms of Me-P*i*PrOx-NH_2 and Me-P*i*PrOx-PBLA. Transmittance changes for 45C52/45A53 in the absence and presence of NaCl. This material is available free of charge via the Internet at http://pubs.acs.org.

LA061431J

(19) Nakayama, M.; Okano, T. *Biomacromolecules* **2005**, *6*, 2320.

Available online at www.sciencedirect.com
ScienceDirect
Journal of Controlled Release 115 (2006) 208–215
journal of controlled release
www.elsevier.com/locate/jconrel

PEGylated gene nanocarriers based on block catiomers bearing ethylenediamine repeating units directed to remarkable enhancement of photochemical transfection

Arnida [a], Nobuhiro Nishiyama [b,c,*], Naoki Kanayama [a,d], Woo-Dong Jang [e], Yuichi Yamasaki [a,c,d], Kazunori Kataoka [a,b,c,d,*]

[a] *Department of Materials Engineering, Graduate School of Engineering, The University of Tokyo, 7-3-1 Hongo, Bunkyo-ku, Tokyo 113-8656, Japan*
[b] *Center for Disease Biology and Integrative Medicine, Graduate School of Medicine, The University of Tokyo, 7-3-1 Hongo, Bunkyo-ku, Tokyo 113-0033, Japan*
[c] *Center for NanoBio Integration, The University of Tokyo, 7-3-1 Hongo, Bunkyo-ku, Tokyo 113-8656, Japan*
[d] *Core Research for Evolutional Science and Technology (CREST) from the Japan Science and Technology Agency (JST), Japan*
[e] *Department of Chemisty, College of Science, Yonsei University, 134 Sinchondong, Seodaemun-gu, Seoul 120-749, Korea*

Received 26 May 2006; accepted 17 July 2006
Available online 20 July 2006

Abstract

The therapeutic usefulness of macromolecular drugs such as plasmid DNA is often limited by the inefficient transfer of macromolecules to the cytosol. Photochemical internalization (PCI) technology, in which the endosomal escape of DNA or its complex is assisted by co-incubated photosensitizers that photodamage endosome membrane, offers a solution for this problem. A series of poly(ethylene glycol) (PEG)-based block polycatiomers with increasing number of ethylenediamine repeating unit at side chain of polycatiomers were complexed with pDNA to form the PEGylated polyplexes as a biocompatible gene carrier. Dendrimeric phthalocyanine (DPc)-incorporated micelle was used to assist the gene transfer of these polyplexes in a light-inducible manner. As a result, the light-inducible transfection activity was significantly enhanced as the number of amino group at the side chain of PEG-*b*-polycatiomer increased. The polyplex from PEG-*b*-polycatiomer having the longest ethylenediamine structure achieved approximately 1000-fold enhancement of transfection upon photoirradiation. This result supports the underlying hypothesis that photochemical transfection and proton sponge effect of polycations can work synergistically to enhance the transfection efficiency. With careful balance between photochemical transfection enhancement and cytotoxicity, PEG-*b*-polycatiomers used in this study might be a potential candidate for *in vivo* PCI-mediated gene transfer.

Keywords: Gene delivery; Polyplex; Polymeric micelle; Photochemical internalization; Photosensitizer

1. Introduction

Gene therapy is a promising approach to conquer intractable diseases for which there is little hope of finding conventional cure. But it still poses several hurdles that need to be overcome before it could enter a clinical phase. Gene therapy mostly depends on the development of the methods for efficient and specific delivery of the gene into the target cells [1–3]. Using viruses as a vector is limited by the safety factor and difficulties in production. By contrast, synthetic gene carriers are versatile and safe, however, its transfection ability might be substantially lower than viral vector [4]. A great deal of challenges in developing non-viral vectors, especially polycatiomer based gene carriers are ongoing in the world.

In non-viral or polycatiomer-mediated gene delivery, endosomal membrane could be a major biological barrier that should be overcome to deliver DNA or its complex to cytosol. In this regard, polyethylenimine (PEI) has been successfully used for the transfection of various types of cells. The early escape of the PEI/DNA complexes from the endosome, arising from "proton

* Corresponding authors. Kataoka is to be contacted at Department of Materials Engineering, Graduate School of Engineering, The University of Tokyo, 7-3-1 Hongo, Bunkyo-ku, Tokyo 113-8656, Japan. Nishiyama, Center for Disease Biology and Integrative Medicine, Graduate School of Medicine, The University of Tokyo, 7-3-1 Hongo, Bunkyo-ku, Tokyo 113-0033, Japan. Tel.: +81 3 5841 7138; fax: +81 3 5841 7139.
E-mail addresses: nishiyama@bmw.t.u-tokyo.ac.jp (N. Nishiyama), kataoka@bmw.t.u-tokyo.ac.jp (K. Kataoka).

0168-3659/$ - see front matter © 2006 Elsevier B.V. All rights reserved.
doi:10.1016/j.jconrel.2006.07.014

sponge effect" was postulated to be the cause of high transfection efficiency [5–7]. However, the polyplexes based on PEI might usually contain an excess of free polymer that is not complexed with DNA. Ultrafiltration or size exclusion chromatography (SEC) can remove free PEI from the polyplexes; however, the purified polyplexes displayed lower transfection efficiency at low DNA concentration [8].

On the other hand, Berg et al. have introduced a novel technology called "photochemical internalization (PCI)", which allows the endosomal escape of the polyplexes in a light-inducible manner. This technology is based upon light activation of photosensitizer specifically locating at the membrane of endocytic vesicles and photochemically disrupting the membrane to release the content from endosome to cytoplasm [9–12]. This method enables the site-specific gene expression in a light-sensitive manner. Indeed, this strategy allowed the light-induced transfection; however, the enhancement of gene expression was accompanied by the photocytotoxicity [11]. The photodamage to sensitive organelles other than endosomal membrane, e.g., the plasma and mitochondrial membranes might be responsible for such photocytotoxicity [13]. Hence, increasing the selectivity of the photodamage to the endosome/lysosome is assumed to lead to the photochemical enhancement of transfection with reduced cytotoxicity. Recently, a ternary complex enveloped with anionic dendrimer phthalocyanine photosensitizer has been developed to achieve the PCI-mediated gene delivery [14]. The ternary complexes showed an expanded range of safe light dose where the photochemical enhancement of the transfection was achieved with a minimal photocytotoxicity, resulting in the success of this system for PCI-mediated gene delivery *in vivo* by local injection [14]. However, this ternary complex system is unlikely to be used for the systemic delivery due to its highly negative charges, which might be recognizable by the scavenger receptor [15]. Hence, it might be required to develop the light-responsive gene carrier applicable for the systemic delivery.

Alternatively, we have developed a biocompatible gene carrier, polyplex micelle based on the micellar assembly of the polyion complex (PIC) with block copolymer consisting poly (ethylene glycol) (PEG) and polycation segments. Their excellent properties for *in vitro* and *in vivo* application have been confirmed such as increased nuclease resistance and high stability under physiological conditions [16,17]. However, the polyplex micelles formed from PEG-*block*-poly(L-lysine) (PEG-*b*-PLL) copolymers possess significantly low transfection ability, which might be due to their inefficient transport from the endosome/lysosome to the cytosol [18]. In this regard, the feasibility of the use of the combination of polymeric micelles incorporating pDNA and dendrimer phthalocyanine (DPc) photosensitizer for PCI-mediated gene delivery has been carried out using PEG-*b*-PLL as carriers. The usefulness of this system for transfection enhancement *in vitro* was successfully demonstrated [19]. This system might be useful for *in vivo* application after systemic delivery. The schematic illustration of this strategy is shown in Fig. 1.

Motivated by this success, we tried to find another vector for pDNA other than PEG-*b*-PLL that might show higher photochemical transfection efficiency. In addition, we also intend to elucidate the structure–photochemical transfection efficiency

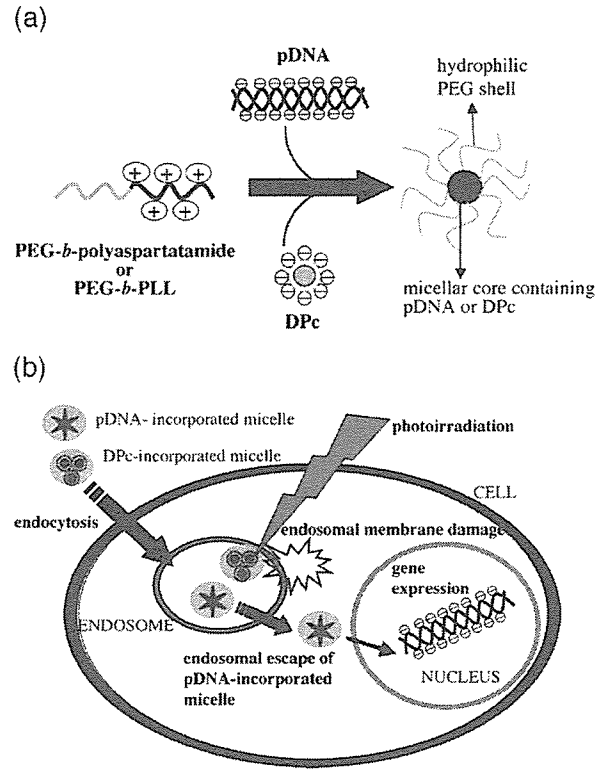

Fig. 1. Schematic illustration of (a) formation of pDNA- and DPc-incorporated micelles through electrostatic interaction between PEG-polycatiomer and pDNA or negatively charged DPc; (b) intracellular trafficking of the pDNA- and DPc-incorporated micelles in the PCI-mediated transfection. Both polymeric micelles are assumed to be taken up by the cell through the endocytic pathway. The localization of the DPc-incorporated micelles in the endosome may allow the selective photodamaging to the endosomal membrane upon photoirradiation, thereby inducing the cytoplasmic delivery of the pDNA-incorporated micelles.

relationship. In the present study, a series of PEG-*b*-polycatiomers bearing a different number of ethylenediamine repeating units at the side chain were used. Recently, we have successfully synthesized PEG-*b*-polyaspartatamide copolymers carrying the ethylenediamine unit at the side chain, which showed an appreciable buffering capacity under endosomal acidic conditions [20]. We hypothesize that the use of buffering polycations may assist the photochemical disruption of the endosomal membrane, thereby accelerating the cytoplasmic delivery of the polyplex micelles upon photoirradiation. The combination of polyplex micelles and DPc micelles was used for PCI-mediated gene transfer in this study.

2. Experimental section

2.1. Materials

N-[*tert*-Butoxycarbonyl (*Z*)]-L-lysine and bis(trichloromethyl)carbonate (triphosgene), for the synthesis of PEG-*b*-PLL diblock catiomers, were purchased from Sigma Aldrich Co., Inc. (St. Louis, MO) and Tokyo Kasei Co., Ltd. (Tokyo, Japan), respectively. β-Benzyl-L-aspartate-*N*-carboxy anhydride (BLA-NCA) and α-methoxy-ω-aminopoly(ethylene glycol)

(MeO-PEG-NH_2, Mw=12 kg/mol) were obtained from Nippon Oil and Fats, Co., Ltd. (Tokyo, Japan). Amine reagents used in aminolysis reaction were purchased from Tokyo Kasei Kogyo, Co., Ltd. (Tokyo, Japan). Chemicals for dendrimer synthesis were purchased from Tokyo Kasei Kogyo and Sigma Aldrich, Co. Inc (St. Louis, MO). *n*-Pentanol and 1,8-diazabicyclo-(5,4,0)-undec-7-ene (DBU) were purchased from Tokyo Kasei Kogyo, and used without further purification. All solvents for the polymer synthesis were distilled before use.

2.1.1. Synthesis of polymers

PEG-*block*-poly(β-benzyl-L-aspartate) (PEG-*b*-PBLA) was prepared according to the previously reported method [20]. PEG-*b*-polyaspartatamide cationers carrying ethylenediamine repeating units at the side chain were prepared through the quantitative aminolysis reaction of PEG-*b*-PBLA in dry DMF at 40 °C for 24 h in the presence of 50-fold molar of ethylenediamine (EDA), diethylenetriamine (DET), triethylenetetramine (TET) and tetraethylenepentamine (TEP) according to the previously reported method [20]. The details of the synthetic procedures and the confirmation of the chemical structures of the synthesized PEG-*b*-polycation copolymers are shown in Figs. S1, S2, S3, S4, S5 and Table S1 in Supporting information.

Synthesis of ionic dendrimer phthalocyanine (DPc) was performed according to the method reported by Ng's group [21]. The second generation of dendritic phenol was reacted with 4-nitrophthalonitrile by an alkali-mediated coupling reaction to obtain the corresponding dendritic phthalonitrile, which was then treated with Zn $(OAc)_2$ and DBU in *n*-pentanol to give the dendrimer phthalocyanine. The dendrimer phthalocyanine thus obtained was treated with a THF/H_2O mixture solution containing NaOH to obtain ionic dendrimer phthalocyanine (DPc; Mw: 4904). The chemical structure of DPc was shown in Fig. 2c.

2.1.2. Preparation of DPc-incorporated polyion complex

The given amount of DPc and PEG-*b*-PLL (Mw of PEG=12,000, repeating unit of PLL=49) (Fig. 2b) was separately dissolved in NaH_2PO_4 (10 mM, pH 4.81 and Na_2HPO_4 (10 mM, pH 9.20) solutions, respectively, and then mixed at a stoichiometric ratio to give a final concentration of DPc 1 mg/ml [22]. The resulting micelle is spherical, with a diameter of ca. 50 nm and narrow size distribution [22].

2.1.3. Preparation of pDNA-incorporated polyplex micelles

Block copolymer and plasmid pCAcc+Luc (pDNA) [23] were dissolved separately in 10 mM Tris–HCl buffer (pH 7.4). Then, polymer solution was added to pDNA solution at a fixed concentration (50 μg/ml) to form complex with various N/P ratios. N/P ratio is defined as the ratio of molar concentration of cationic moieties in diblock cationer to that of phosphate group in pDNA. Final concentration of pDNA was fixed at 33.3 μg/ml. Complexes were kept at room temperature overnight before use.

2.1.4. Dynamic light scattering measurement

The size of pDNA polyplex micelles was evaluated by dynamic light scattering (DLS) measurement. Sample solutions

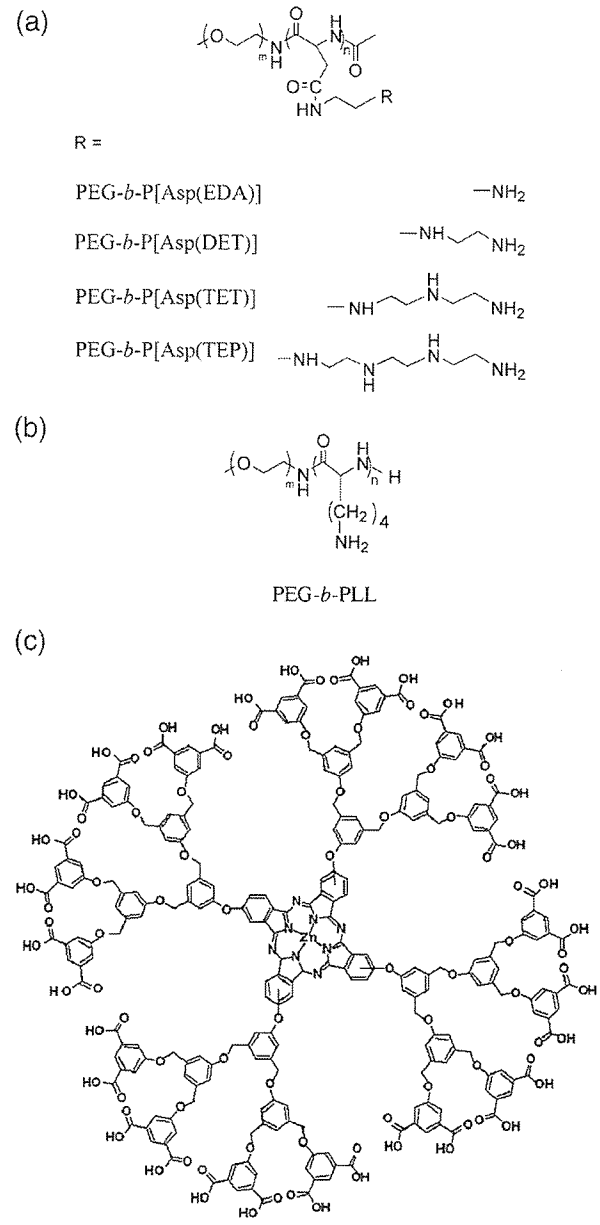

Fig. 2. (a) Chemical structures of PEG-*b*-P[Asp(EDA)], PEG-*b*-P[Asp(DET)], PEG-*b*-P[Asp(TET)], and PEG-*b*-P[Asp(TEP)]; (b) chemical structure of PEG-*b*-PLL; (c) chemical structure of anionic dendrimer phthalocyanine (DPc).

with various N/P ratios in 10 mM Tris–HCl buffer (pH 7.4) were adjusted to pDNA concentration of 33.3 μg/ml. DLS measurements were carried out at 25.0±0.2 °C using a DLS-7000 instrument (Otsuka Electronics, Osaka, Japan) with a vertically polarized incident beam of 488 nm wavelength from an Ar ion laser. A scattering angle of 90° was used in these measurements. Data were analyzed by a cumulant method as reported in detail previously [24].

2.1.5. Laser-doppler electrophoresis measurement

Laser-doppler electrophoresis measurements were carried out using a ELS-6000 (Otsuka Electronics Co., Ltd., Osaka, Japan) at 25 °C. From the electrophoretic mobility, the zeta

potential (ζ) was calculated using Smoluchowski equation as follows:

$$\zeta = 4\pi\eta u/\varepsilon$$

where u is the electrophoretic mobility, η is the viscosity of the solvent, and ε is the dielectric constant of the solvent.

2.1.6. Ethidium bromide exclusion assay

The effect of the N/P ratio on the degree of pDNA condensation in PIC micelle was estimated from the reduction in fluorescence intensity of ethidium bromide (EtBr) due to the exclusion from DNA. PIC micelle solutions (33.3 μg of pDNA/mL) prepared at various N/P ratios were adjusted to 20 μg of pDNA/mL with 0.4 μg of EtBr/mL by adding 10 mM Tris–HCl buffer containing EtBr. The ratio of residual molar concentration of EtBr to that of the base pair in pDNA was 0.033. The solutions were incubated at ambient temperature overnight. Fluorescence measurement of sample solution was carried out at 25±0.2 °C using a spectrofluorometer (JASCO, FP-6500). Excitation (Ex) and emission (Em) wavelengths were 510 and 590 nm, respectively. Results were expressed as relative fluorescence intensity. The fluorescence of pDNA solution with EtBr was set at 100%, and measured against a background of EtBr without pDNA.

2.1.7. Cell culture and photochemical transfection

Human hepatoma Huh7 cells were cultured in DMEM containing 10% fetal bovine serum (FBS) and 10 mM HEPES buffer. The cells were grown at 37 °C in humidified atmosphere containing 5% CO_2. In the experiment, 10,000 cells per well were plated on 24-well plate 24 h before transfection. The cells then were incubated in a medium containing DPc-loaded micelles and pDNA polyplex micelles prepared at an N/P ratio of 2. The amount of pDNA was adjusted to 1 μg per well while DPc concentrations were varied. After 6 h incubation at 37 °C, the medium was replaced with fresh medium to remove non-associated photosensitizers. The cells then were irradiated for 45 min (except for irradiation times variation experiment) using halogen lamp equipped with a band-pass filter (400–700 nm) at a fluence rate of 3 mW/cm^2. After another 48 h incubation at 37 °C, the luciferase gene expression was measured using LB940, Berthold Technologies (Bad Wilbad, Germany). The amount of protein in each well was determined using Micro BCA Protein Assay Reagent Kit, Pierce Chemical Co., Inc. (Rockford, USA).

2.1.8. Cytotoxicity measurement

Cell culture was carried out as described above. After 48 h incubation, the viability of the cells was evaluated using 3-(4,5-dimethylthiazol-2-yl)-2,5-diphenyltetrazolium bromide (MTT) assay [25]. Briefly, 40 μl of MTT solution (5 mg/ml in PBS) was added to each well, followed by 4 h incubation at 37 °C. Then, 400 μl SDS solution (20% w/v in PBS) was added to dissolve the formed formazan. After 2 days incubation at room temperature, the absorbance from each well was measured at 570 nm. Results were expressed as percentage relative to control.

3. Results and discussion

The PEG-*b*-polyaspartatamide catiomers with different amino functionality at the side chain used for pDNA delivery were synthesized through the new synthetic procedure of PEG-*b*-polycatiomer developed in our laboratory [20]. It based on the recent finding that the benzyl ester group of poly(β-benzyl-L-aspartate) (PBLA) can undergo aminolysis reaction with the primary amino group of polyamine compounds in a selective and quantitative manner under a mild condition, allowing the preparation of cationic polyaspartatamides with different amino functionality but the same molecular weight. In our previous study, we found that PEG-*b*-polycatiomer having the ethylenediamine structure at the side chain showed sufficient buffering

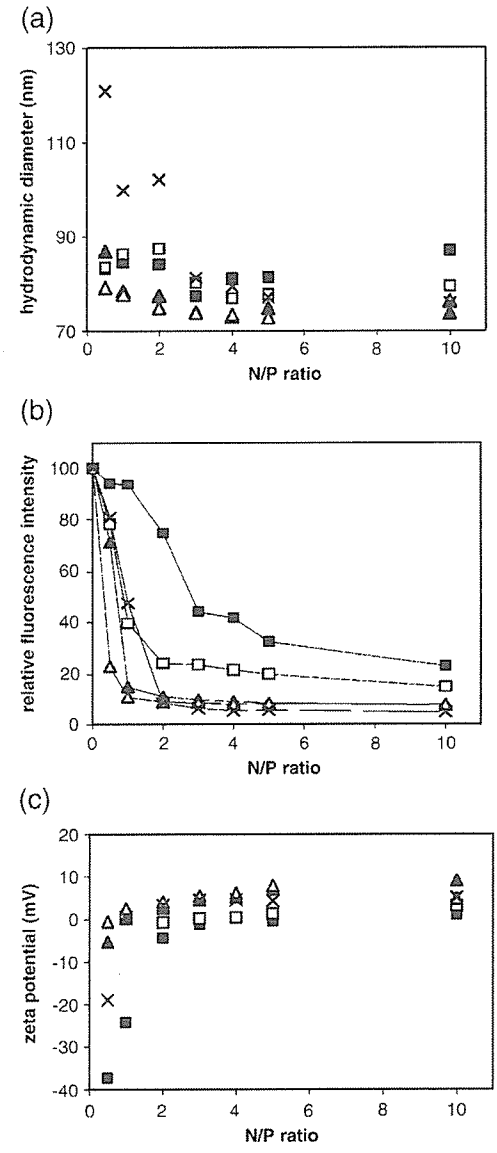

Fig. 3. Properties of PEG-*b*-polycation/pDNA polyplex micelles: (a) change in the cumulant diameter, (b) fluorescence intensity of EtBr and (c) zeta potential value of the polyplexes prepared at different mixing ratios. (■) PEG-*b*-P[Asp(EDA)]; (□) PEG-*b*-P[Asp(DET)]; (▲) PEG-*b*-P[Asp(TET)]; (△) PEG-*b*-P[Asp(TEP)]; (×) PEG-PLL.

capacity and therefore enhanced transfection efficiency based on the aforementioned proton sponge effect [20]. In this study, we hypothesized that the use of the buffering polycations might facilitate the PCI-mediated gene delivery, and aimed to optimize the chemical structure of PEG-*b*-polycatiomers for this purpose. Therefore, we synthesized a series of PEG-*b*-polycatiomers carrying the ethylenediamine repeating units (PEG-*b*-P[Asp (EDA)]), PEG-*b*-P[Asp(DET)], PEG-*b*-P[Asp(TET)] and PEG-*b*-P[Asp(TEP)]) at the side chain with fixed composition of 12–68 (Mw of PEG=12,000, repeating unit of cationic segment=68). The chemical structures of these block catiomers were confirmed by ^{1}H NMR and size exclusion chromatography measurements (Figs. S1, S2, S3, S4, S5 and Table S1 in Supporting information), and are shown in Fig. 2a.

The polyplex micelles were prepared by mixing the solution of each polymer and pDNA at various N/P ratios. The size of the polyplexes was then evaluated by DLS measurement. The hydrodynamic diameter of the polyplexes was revealed to be 70–90 nm through the range of examined N/P ratios as shown in Fig. 3a. Increasing N/P ratio decreases the hydrodynamic diameter of the polyplexes, suggesting the formation of more compact pDNA micelles probably due to the increased densities of positive charges surrounding pDNA polyplexes. From the practical point of view, the polyplex micelles need to be stable under physiological salt concentrations. Therefore, the DLS measurements of the polyplex micelles were carried out after 24-h incubation in 150 mM NaCl solutions. Consequently, the polyplex micelles maintained the particle size of 100 nm with a narrow distribution above the N/P ratio of 2.0, whereas the branched polyethylenimine (BPEI) polyplexes showed appreciable increases in the particle size and polydispersity index (Fig. S6 in Supporting information). This result suggests high stability of polyplex micelles under physiological conditions for *in vivo* use.

Ethidium bromide (EtBr) is a DNA intercalator and exhibits approximately 10-fold greater fluorescence emission upon binding to DNA. Condensation of DNA by cationic component displaces EtBr, resulting in the reduced fluorescence intensity. Hence, EtBr exclusion assay was frequently used to estimate the degree of pDNA condensation in polyplexes [26]. We found that in the order of PEG-*b*-P[Asp(EDA)], PEG-*b*-P[Asp(DET)], PEG-*b*-P[Asp(TET)] and PEG-*b*-P[Asp(TEP)], pDNA condensation ability increased (i.e., the N/P ratio required to reduce the EtBr fluorescent intensity decreased) as shown in Fig. 3b. It seems that longer polyamine side chain more effectively interacts with DNA double strands, thereby replacing the dye molecule. Except for PEG-*b*-P[Asp(EDA)], all the PEG-*b*-polycatiomers induced EtBr quenching to be leveled off at N/P ratio of 2, suggesting the completion of pDNA condensation at N/P ratio less than 2. PEG-*b*-P[Asp(EDA)]/pDNA polyplex retained 75% of its fluorescence intensity at N/P ratio of 2. As known, P[Asp(EDA)] has shorter spacer between the primary amino group and backbone polymer, and this may explain the lower condensation ability of DNA.

Zeta potential values of the polyplex micelles increased with increasing N/P ratio and were almost leveled off at N/P ratio of 2 (Fig. 3c). EtBr exclusion assay also indicated that at N/P ratio

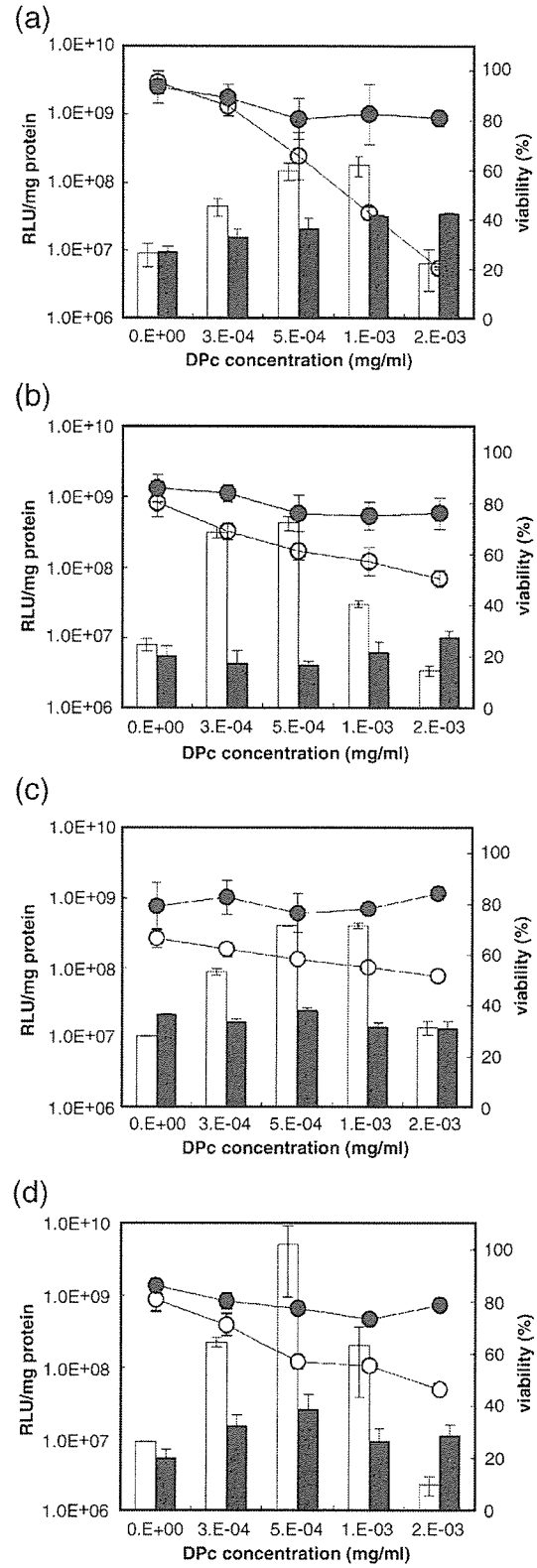

Fig. 4. The effect of DPc concentration on the transfection efficiency and cytotoxicity of the PCI-mediated transfection using the combination of pDNA- and DPc-incorporated micelles. (a) PEG-*b*-P[Asp(EDA)], (b) PEG-*b*-P[Asp (DET)], (c) PEG-*b*-P[Asp(TET)] and (d) PEG-*b*-P[Asp(TEP)] as pDNA vector. Open bar: transfection efficiency with irradiation; solid bar: transfection efficiency without irradiation; ○: photocytotoxicity; ●: dark cytotoxicity.

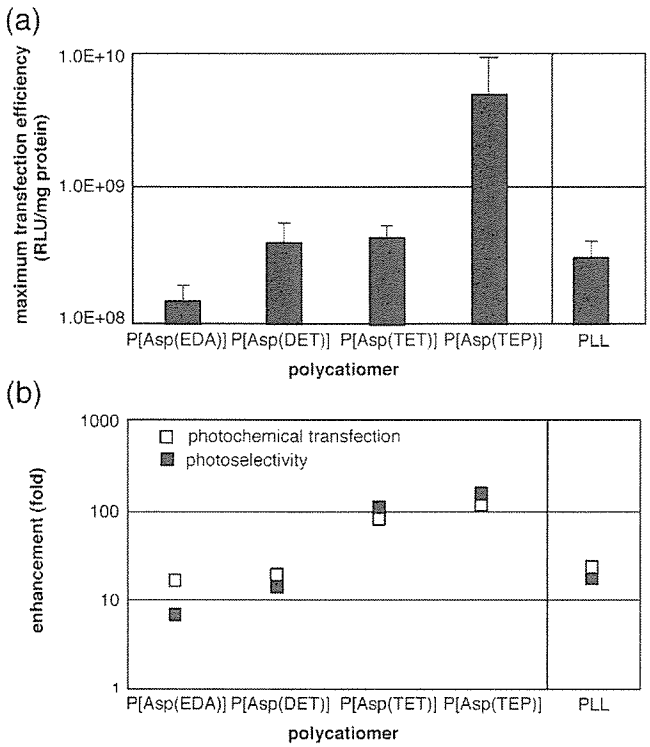

Fig. 5. Comparison of (a) transfection efficiency and (b) photochemical transfection enhancement and photoselectivity at optimal DPc concentration between the polyplex micelles from PEG-*b*-P[Asp(EDA)], PEG-*b*-P[Asp (DET)], PEG-*b*-P[Asp(TET)], PEG-*b*-P[Asp(TEP)] and PEG-*b*-PLL.

of 2, the pDNA was fully condensed in the core. A gradual increase of the zeta potential suggests adsorption of polymer onto the polyplex surface. Above N/P ratio of 2, the polyplexes have relatively small absolute zeta potential values, suggesting the formation of the core-shell structured polyplex micelles covered with PEG palisades. The sterically repulsive character of the neutral PEG layers prevents the micelles from secondary aggregation, keeping their highly dispersive nature in aqueous medium. These characters are expected to provide the polyplexes with prolonged blood circulation by avoiding interaction with serum proteins and cellular components [17]. Another advantage of the presence of neutral PEG layers at the outer part of the micelle might be the minimization of toxicity of the polycatiomers due to its binding with various types of RNA and genomic DNA that impairs the normal cellular functions of these polyanions [27].

In this study, the PCI using polymeric micelles incorporating dendrimer-based photosensitizers [dendrimer phthalocyanine (DPc) illustrated in Fig. 2c] was carried out to enhance the gene transferring ability of the aforementioned polyplex micelles in a light-selective manner. DPc has longer excitation wavelengths (i.e., strong Q-band absorptions at 630 and 685 nm), facilitating deeper tissue penetration of light therefore preferable for clinical use [28,22]. The rationale for the use of polymeric micelles as a nanocarrier of DPc is similar to that for the delivery of DNA, which are to prolong blood circulation after intravenous administration and to selectively accumulate them in the target tissues such as solid tumors as previously reported [22,29,30]. Also, both micelles are assumed to show the same subcellular localization in the endosome due to similar particle sizes and surface properties, which might be a key to success in the PCI-mediated gene delivery [14,19].

To evaluate the ability of the combinatorial use of the newly developed polyplex micelles and DPc-incorporated micelles for the PCI-mediated gene delivery, *in vitro* transfection was performed on human hepatoma Huh7 cells with a luciferase (Luc) reporter gene in the presence and absence of photoirradiation. The photochemical transfection and cytotoxicity were examined using the combination of polyplex micelles at N/P ratio of 2, where the fluorescence intensity was found to be leveled off for most of the complexes (Fig. 3b), and the DPc-incorporated micelles with different concentrations of DPc. The photoirradiation was carried out using a broad band light of 400–700 nm with 3 mW/cm^2 of fluence rate for 45 min. The PCI-mediated gene transferring ability and cytotoxicity of the polyplexes from PEG-*b*-P[Asp(EDA)], PEG-*b*-P[Asp(DET)], PEG-*b*-P[Asp(TET)] and PEG-*b*-P[Asp(TEP)] are shown in Fig. 4a, b, c and d, respectively. All the polyplexes showed the photochemical enhancement of the gene expression with optimum doses of DPc ($5*10^{-4}$ mg/ml), above in which the transfection efficiency decreased. The decrease of transfection efficiency with increasing DPc concentration is most likely to be caused by increased photocytotoxicity (open symbols in Fig. 4). Hence, the PCI-mediated transfection with the DPc-incorporated micelles should be performed based on a careful balance between transfection efficiency and cytotoxicity. But there is also another possibility that the lowered transfection may be due to the damage of the plasmid DNA induced by photochemical treatment [31].

The maximum transfection efficiencies achieved by the PCI-mediated gene delivery using polyplex micelles from different block catiomers are summarized in Fig. 5a. Also, the photochemical transfection enhancement and photoselectivity are shown in Fig. 5b. Photochemical transfection enhancement is defined as the ratios of the above-mentioned maximum transfection efficiency to the transfection efficiency of the polyplex

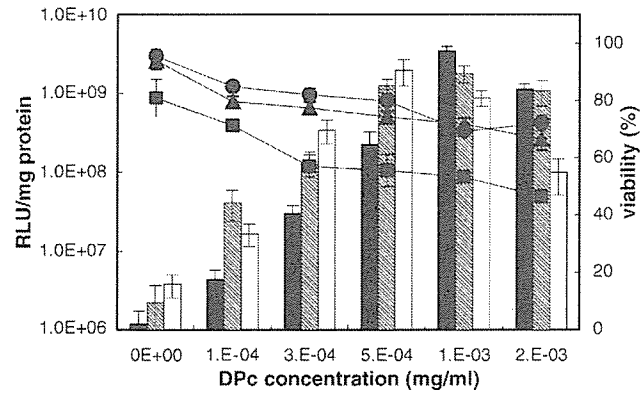

Fig. 6. The effect of irradiation times on photochemical transfection [solid bar: 20 min; hatched bar: 30 min; open bar: 45 min irradiation] and photocytotoxicity [●: 20 min; ▲: 30 min; ■: 45 min irradiation] of PEG-*b*-P[Asp(TEP)] polyplex micelle at different DPc concentrations.

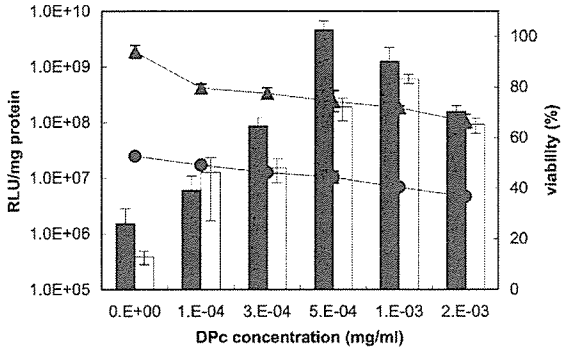

Fig. 7. Comparison of photochemical transfection efficiency (solid bar: BPEI; open bar: PEG-*b*-P[Asp(TEP)]) and photocytotoxicity (●: BPEI; ▲: PEG-*b*-P[Asp(TEP)]) between the polyplex micelles from PEG-*b*-P[Asp(TEP)] and BPEI 25 kDa at various concentrations of DPc and 20 min irradiation.

micelles alone, while photoselectivity is the ratios of the maximum PCI-mediated transfection efficiency to the transfection efficiency of the combination of the pDNA- and DPc-incorporated micelles without photoirradiation. As shown in Fig. 5a, increasing the length of ethylenediamine structure at the side chain of polycation segment of diblock copolymer led to an appreciable increase in the photochemical transfection efficiency even at the same N/P ratio. Also, the polyplexes from PEG-*b*-polyaspartatamide catiomer gave a higher photochemical transfection than those of PEG-*b*-PLL, except for PEG-*b*-P[Asp(EDA)], which lacks both the ability to condense DNA and buffering capacity [20]. Notably, PEG-*b*-P[Asp(TEP)] bearing 3 times-repeated ethylenediamine units showed a 1000-fold photochemical transfection enhancement, which is in a marked contrast with those obtained by PEG-*b*-P[Asp(TET)] bearing 2 times-repeated ethylenediamine units (76-fold) and PEG-*b*-P[Asp(DET)] bearing mono-ethylenediamine unit (19-fold) (Fig. 5b). Thus, the photochemical transfection enhancement of the polyplex micelles increased as the length of the ethylenediamine structure at the side chain of block catiomer strand increased. The mechanisms of the enhanced PCI-mediated transfection dependent on the length of the ethylenediamine side chain remain to be clarified. It is possible that the increasing number of a relatively low pK_a secondary amino groups may contribute to such transfection enhancement. Increasing the length of the ethylenediamine side chain increased the pDNA condensation ability (Fig. 3b), which may also contribute to the enhanced PCI-mediated transfection. However, this factor is unlikely to be solely effective in the photochemical transfection, since PEG-*b*-PLL showed lower PCI-mediated transfection efficiency than those of PEG-*b*-P[Asp(DET)], PEG-*b*-P[Asp(TET)] and PEG-*b*-P[Asp(TEP)] despite its high DNA condensation ability. Thus, as we hypothesized, the use of block catiomers having the ethylenediamine side chain with a high buffering capacity may assist the photochemical disruption of the endosomal membrane due to the proton sponge mechanism [5], thereby accelerating the cytoplasmic delivery of the polyplex micelles upon photoirradition. The synergistic effect between photochemical reaction and proton sponge effect on the PCI-mediated transfection has been successfully demonstrated in this study.

PEG-*b*-P[Asp(TEP)] gave the highest and remarkable photochemical transfection enhancement. In this experiment, the effect of the irradiation times on the PCI-mediated transfection using polyplex micelles from PEG-*b*-P[Asp(TEP)] was further studied. In particular, we tried to find an optimum irradiation condition for high transfection enhancement without a trade on the viability of the cells. Fig. 6 shows the photochemical transfection and photocytotoxicity of PEG-*b*-P[Asp(TEP)] polyplex micelle at different irradiation times. As the irradiation time increased, the optimum condition for photochemical transfection was shifted to a lower concentration of DPc while the photocytotoxicity increased. The highest photochemical transfection enhancement was achieved at DPc concentration of 0.001 mg/ml and irradiation times of 20 min with around 72% of the cells remained alive. Thus, this condition might be an optimum irradiation condition for photochemical transfection enhancement for PEG-*b*-P[Asp(TEP)] polyplex micelle.

Further, polyethylenimine (PEI) consisting of ethylenediamine units, which is one of the most highly transfectable polycatiomers, was used as pDNA vector for the PCI-mediated transfection. In this study, we compared the photochemical transfection efficiency and photocytotoxicity between PEG-*b*-P[Asp(TEP)] and 25 kDa branched PEI (BPEI) as pDNA vector (Fig. 7). BPEI showed approximately 7-fold higher transfection enhancement compared to PEG-*b*-P[Asp(TEP)] at the optimum DPc concentration. Nevertheless, the transfection with BPEI was accompanied by significant cytotoxicity. The PEG-*b*-P[Asp(TEP)] polyplex micelle showed significantly lower cytotoxicity despite its efficient PCI-mediated transfection ability.

In conclusion, we have studied on the relationship between chemical structure of block catiomers and photochemical transfection efficiencies. The light-inducible transfection activity was significantly enhanced as the length of the ethylenediamine side chain of PEG-*b*-polycatiomer increased. PEG-*b*-P[Asp(TEP)] gave the highest photochemical enhancement and photoselectivity of the transfection. The PEG-*b*-polyaspartatamide catiomers, except for PEG-*b*-P[Asp(EDA)], are more effective than PEG-*b*-PLL, which was used in the previous study [19], as a pDNA vector for the light-selected gene transfer. It is worth mentioning that all the polyplex micelles used in this study were prepared under the conditions with minimal free polymers (i.e., at the N/P ratio of 2.0), facilitating their use for the systemic administration. PEG-*b*-polyaspartatamide catiomers as pDNA vector might become vectors for the PCI-mediated gene transfer *in vivo* after systemic delivery.

Acknowledgments

The authors wish to express their gratefulness to the Health and Labor Sciences Research Grants in Research on Advanced Medical Technology in Nanomedicine Area from the Ministry of Health, Labor and Welfare (MHLW), Japan. Also, they wish to express their thanks to the Project on the Materials Development for Innovative Nano-Drug Delivery Systems from the Ministry of Education, Culture, Sports, Science and Technology (MEXT), Japan.